




Universitat Autònoma de Barcelona

 *Chemical Transducers Group (GTQ)*

 *Institut de Microelectrònica de Barcelona (IMB-CNM)*

 *Consejo Superior de Investigaciones Científicas (CSIC)*

Programa de Doctorat en Física
Thesis submitted to obtain the degree of Doctor in Philosophy

Living Photonics: Lab-on-a-chip technologies for light coupling into biological cells

Doctoral Dissertation of:
Tobias Nils Ackermann

Supervisors:
Dr. Andreu Llobera Adàn

and
Dr. Xavier Muñoz Berbel

Tutor:
Prof. Dr. Verònica Ahufinger

September 2017

A.1 Publications directly related to this thesis

A.1.1 Journal articles

- Isaac Rodríguez-Ruiz, Tobias N. Ackermann, Xavier Muñoz-Berbel, and Andreu Llobera. Photonic Lab-on-a-Chip: Integration of Optical Spectroscopy in Microfluidic Systems. *Analytical Chemistry*, 88(13):6630–6637, 2016. ISSN 15206882. doi: 10.1021/acs.analchem.6b00377. URL <http://dx.doi.org/10.1021/acs.analchem.6b00377>
- Tobias Nils Ackermann, Pablo Giménez-Gómez, Xavier Muñoz-Berbel, and Andreu Llobera. Plug and measure – a chip-to-world interface for photonic lab-on-a-chip applications. *Lab Chip*, 16(17):3220–3226, 2016a. ISSN 1473-0197. doi: 10.1039/C6LC00462H. URL <http://xlink.rsc.org/?DOI=C6LC00462H>
- Lightguiding through biofilms: optical sensing of microbial surface colonization on-chip (In preparation)

A.1.2 Conferences

- Cristina Rius, Tobias N. Ackermann, Beatriz Dorado, Xavier Muñoz-Berbel, Vicente Andrés, and Andreu Llobera. Fiber optic label-free biophotonic diagnostic tool for cardiovascular disease. In Sander van den Driesche, editor, *Progress in Biomedical Optics and Imaging - Proceedings of SPIE*, volume 9518, page 95180V. SPIE, jun 2015. ISBN 9781628416411.

doi: 10.1117/12.2179062. URL <http://proceedings.spiedigitallibrary.org/proceeding.aspx?doi=10.1117/12.2179062>

- D. King, E. Røge Hedegaard, Tobias Nils Ackermann, C. Rius, X. Muñoz-Berbel, H. Knudsen, I. Rodríguez-Rodríguez, B. Dorado, E. Alvarez, J. Ducrée, V. Andrés, U. Simonsen, and A. Llobera. Living photonics: Monitoring light propagation through cells (LiPhos). *Progress in Biomedical Optics and Imaging - Proceedings of SPIE*, 9518:1–7, 2015. ISSN 16057422. doi: <http://dx.doi.org/10.1117/12.2181306>
- Tobias Nils Ackermann, Erica Álvarez-Conde, Pere Jiménez-Benet, Andreu Llobera, Xavier Muñoz-Berbel. Transfer of SU-8 waveguides from silicon wafers to thermoplastic polymethylmetacrylate (PMMA) substrates for all-polymer photonic lab-on-a-chip devices. (Abstract accepted for poster presentation at *MNE: International Conference on Micro- and Nanoengineering*, Braga, Portugal 2017)

The two already published articles are reprinted following.

A.1.3



Lab on a Chip

TECHNICAL INNOVATION

Cite this: *Lab Chip*, 2016, 16, 3220

Plug and measure – a chip-to-world interface for photonic lab-on-a-chip applications†

Tobias Nils Ackermann,* Pablo Giménez-Gómez,
Xavier Muñoz-Berbel and Andreu LloberaReceived 6th April 2016,
Accepted 30th June 2016

DOI: 10.1039/c6lc00462h

www.rsc.org/loc

The integration of detection mechanisms with microfluidics may be one of the most promising routes towards widespread application of Lab-on-a-Chip (LoC) devices. Photonic detection methods like in the so-called Photonic Lab-on-a-Chip (PhLoC) have advantages such as being non-invasive, easy to sterilize and highly sensitive even with short integration times and thus allow *in situ* monitoring and quantification of biological and chemical processes. The readout of such detection methods usually requires special training of potential users, as in most cases they are confronted with the need of establishing fiber-optics connections to and from the PhLoC and/or rely on the use of complex laboratory equipment. Here, we present a low-cost and robust chip-to-world interface (CWI), fabricated by CO₂-laser machining, facilitating the non-expert use of PhLoCs. Fiber-optics with standard SMA-connectors (non-pigtailed) and PhLoCs can be plugged into the CWI without the need for further adjustments. This standardization bestows great versatility on the interface, providing a direct link between PhLoCs and a wide range of light sources and photo-detectors. The ease-of-use of the proposed simple plug mechanism represents a step forward in terms of user-friendliness and may lead PhLoC devices to practical applications.

1 Introduction

The field of microfluidics and Lab-on-a-Chip (LoC) has been envisioned to have tremendous potential to produce high-throughput analytical tools for pharmaceutical and biotech research^{1,2} as well as practical devices for point-of-care (PoC) diagnostics, performing complex laboratory procedures on a microchip. A variety of microfluidic platforms have been developed in the past decade to control liquid movement on-chip³ through components like micro-pumps,^{4,5} -valves⁶ and -mixers.^{7–9} Also, different detection schemes such as electrochemical¹⁰ or optical measurements^{11–13} in microfluidics have been validated in proof-of-concept studies, showing their potential advantages over laboratory tests.^{3,14,15} Still, only a small percentage of published research based on LoCs and microfluidics has reached the stage of actual implementation as a technology that aids biologists in their everyday research¹⁶ or achieved successful introduction into the market as consumer products.^{17,18}

The main obstacle regarding the practical, user-friendly implementation of LoCs with any detection scheme remains

in the development of robust connections from the device to the outside world (hereafter named ‘interface’), allowing effective handling also by non-experts.^{19,20} Regarding fluidic handling, a variety of robust connectors have been reported during the past decade.^{19,21–23} Companies like *microfluidic ChipShop*, *Cellix* or *Dolomite*²⁴ offer entire series of already functionalised LoCs with fluidic connectors directly attached to and compatible with their respective pumping systems. Most of the current commercialization models are directed towards a business-to-business (B2B) strategy involving the research and academic market instead of the development of a real end-user product.²⁵ Developers are now moving away from the idea of a single ‘killer app’ and are instead focusing their efforts on bridging the divide between industry and academia in the hopes of using microfluidics as an enabling technology for a wide range of life-science applications.²⁴

As one of the pursued development paths towards enhancing functionality, the integration of optical/optoelectronic elements with microfluidics has resulted in a new generation of highly sensitive and robust bio-sensors.^{12,13,15} Optical detection schemes have advantages such as being non-invasive, easy to sterilize and potentially highly sensitive even with short integration times. This makes them particularly useful not only for monitoring of biological processes in applications like bio-assays and on-site monitoring in environmental studies but also for PoC diagnostics, where an immediate result is desired by the end-user.

Institut de Microelectrónica (IMB-CNM), Campus UAB, E-08193 Cerdanyola del Vallès, Spain. E-mail: tobias.ackermann@imb-cnm.csic.es; Fax: +34 93 580 1496; Tel: +34 93 594 7700 (ext. 2431)

† Electronic supplementary information (ESI) available. See DOI: 10.1039/c6lc00462h

While active components like photo-diodes promise fully incorporated detection and readout, such integration with the microfluidic platform is technologically challenging and expensive and in most examples^{26–30} either the light source or detection remains ‘off-chip’¹¹ or needs external stimuli (e.g. pumping lasers) for the integrated units to work.

Alternatively, the integration of passive photonic elements with microfluidics, as in the so-called Photonic Lab-on-a-Chip (PhLoC),³¹ offers greatly simplified fabrication processes, as photonic and fluidic components can be defined in the same step and using low-cost materials and processes. They would therefore be more suitable for PoC applications in the form of disposable cartridges. On the downside, potential users are confronted with the need to use external bulk optics and establish optical (and probably fluidic) connections to and from the PhLoC. Since microfluidic devices are often only used a few times, typically only one to avoid cross-contamination, it would be desirable to easily insert (or replace) them in a holder (the ‘interface’), where the fluidic, optical and maybe even electrical connections are made without any active alignment by the user.¹² Yet, for photonic applications, to our knowledge, no such interface has been presented to the scientific community to date.

In this work, we focus on this open issue and present a robust chip-to-world interface (CWI) fabricated and assembled by low-cost methods to facilitate fiber-optics coupling to PhLoCs for non-expert users. After introducing the involved design schemes and fabrication methodology, we compare the performance of the low-cost fiber-coupler to that of a commercial counterpart and present an experimental study exploring the robustness and required alignment margins of the fully assembled CWI.

2 Design and working principle

Fig. 1a shows an emulator of a PhLoC only comprising a bent dielectric waveguide (WG) on a transparent substrate, which

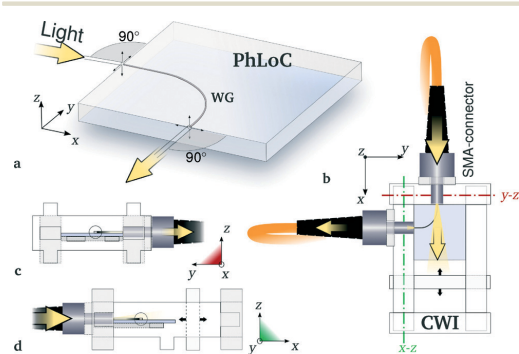


Fig. 1 a) Illustration of a PhLoC emulator comprising a 90° bent dielectric waveguide, b) schematic top-view of CWI with PhLoC and SMA fiber-connectors plugged-in, c) schematic of the input-plane depicting the positioning of the waveguide input facet aligned with ‘plug-optics’ connector, d) equivalent schematic of the output plane. Light coupling and propagation is indicated by arrows throughout the schemes a)–d).

will serve as a model for a proof-of-concept. As illustrated, effective coupling to and from the WG occurs at specific relative coordinates and incident angles of 90° to the respective edges of the PhLoC.

The proposed chip-to-world interface (CWI) for such PhLoCs is depicted in Fig. 1b–d. The required precise relative positioning of fiber-optics connections and PhLoC is achieved by splitting the design scheme in several independent building blocks. That way, every unit can be fabricated separately in-plane, which makes it possible to take advantage of the full lateral resolution of the planar technologies used in this work. As shown in Fig. 1b, a robust outer frame composed of four interlocked blocks confines the PhLoC in the y-axis. To facilitate the insertion and removal of the PhLoC, an additional movable block is used to confine the space in the x-direction and push the PhLoC in position after insertion – aligned with the fiber-optics (more information on the concrete building block design used in this work can be found in Fig. S1 and S3, ESI†). Fig. 1b and c depict the design schemes of the blocks for the input (y–z) and output (x–z) planes, respectively. A thin platform is anchored here at the required height level (z-position) to align the end-facets of the WG with the center of the circular opening representing the fiber-connector. The fiber connections are optimized to facilitate plugging in and out of industrial standard SMA-connectors in order to increase the versatility and ease-of-use of the interface. As those connectors have standardized dimensions, the user can choose among a variety of fiber diameters without changing the design. A detailed model of the proposed fiber connections (hereafter called ‘plug-optics’) can be found in Fig. S1, ESI†.

The design of the CWI and the photonic structures on the PhLoC is coupled and based on the idea of trading coupling losses for a high signal-to-noise ratio. Concretely, we introduce the 90° bends in the WGs to achieve an optical output perpendicular to the optical input. In this way, independent of the in-coupling efficiency, the output will result from the light coupled into the photonic structure of the PhLoC (signal), while the non-confined light (noise) should not reach the readout. This approach allows us to use integrated photonic structures with far smaller dimensions than those of the input fiber-optics without spoiling the signal-to-noise ratio. Thus, the required alignment precision can be met by low-cost (and high-throughput) fabrication while maintaining full functionality.

3 Materials and methods

3.1 Materials

SU-8 2005 was purchased from MicroChem Corp. and used as-received. 4" borosilicate wafers were purchased from SCHOTT AG with a thickness of 0.7 mm. PMMA plates were purchased from Ferreteria Maranges S.A. with thicknesses of 1 mm, 3 mm and 5 mm, and flexible polyurethane foam was purchased from RS Components Ltd.

3.2 PhLoC fabrication

For the fabrication of the dielectric waveguides, a 6 μm thick SU-8 layer was spin-coated at 3000 rpm on O₂ plasma-activated borosilicate (Pyrex®) wafers. The 90 μm wide waveguides (bend radius = 4 mm) were then defined *via* direct photo-lithography (see the ESI† for details), resulting in a WG cross-section of $90 \times 6 \mu\text{m}^2$. The wafer was cut using a diamond blade cutting machine (safety distance $\equiv 25 \mu\text{m}$ from the WG facets) to release the individual PhLoCs.

3.3 CO₂ laser processing

The CWI building blocks were fabricated *via* CO₂ laser processing of poly-methyl methacrylate (PMMA), which combines the attributes low cost and minimum time consumption (being a one-step process). Thus, it is an ideal method for rapid prototyping as well as industrial level fabrication of the final product.

PMMA, while being highly transparent in the visible spectrum, acts as an excellent absorber in the far infrared region and can therefore be very effectively processed using a CO₂ laser. In addition, its low weight, reasonable hardness and low cost are perfect characteristics for a cheap and robust CWI.

In this work, we used a commercially available Epilog Mini 24 laser writer employing a CO₂ laser (see Table 1 for specifications) for the fabrication. It can be directly addressed by a computer as one would a conventional printer. 2D patterns designed as vector graphics are sent to the machine together with the desired configurations of power (P), writing speed (S) and laser pulse frequency (F). The combination of the latter parameters controls the Gaussian beam shape of the laser and thus the line-width as a function of the penetration depth as described elsewhere.³²

For the fabrication of the CWI building blocks, 1 mm, 3 mm, and 5 mm thick PMMA sheets were employed. With increasing thickness of PMMA, the variation of the line-width as a function of depth becomes more important, resulting in a measurable difference between the line-widths d_{top} at the top and d_{bottom} at the bottom of the PMMA sheet. Thus, the cutting conditions have been optimized for the 3 mm and 5 mm thick PMMA sheets with the aim to minimize this variation (compare Fig. S4, ESI†) and achieve vertical walls. We found that due to different mechanisms for the motion control in the x - and z -axes of the laser writer, the average line-width $\bar{d} = (d_{\text{top}} + d_{\text{bottom}})/2$ also differs depending on the direction of the cut (see Table 2).

3.3.1 CWI assembly. The crucial part for robust interlocks between adjoining building blocks is the corresponding plugs and sockets. The relative dimensions were empirically opti-

Table 2 Cutting conditions and the corresponding line-widths for PMMA as used in the fabrication of the CWI elements. F is the laser pulse frequency in Hz, P is the percentage of maximum power and S is the percentage of maximum speed. The full characterization can be found in the ESI

PMMA thickness	Conditions	Resulting average line-width \bar{d}
5 mm	$F = 5000$	$\bar{d}_x = 160 \mu\text{m} \pm 30 \mu\text{m}$
	$P = 100$	$\bar{d}_y = 220 \mu\text{m} \pm 25 \mu\text{m}$
	$S = 5$	
3 mm	$F = 5000$	$\bar{d}_x = 235 \mu\text{m} \pm 20 \mu\text{m}$
	$P = 100$	$\bar{d}_y = 195 \mu\text{m} \pm 10 \mu\text{m}$
	$S = 7$	

mized under consideration of the previous characterization of direction-dependent line-width as shown in Fig. 2a. For the best fitting of adjoining parts, a tolerance value of 150 μm was added to the desired dimension in x or y according to $w_{\text{design}} = w_{\text{real}} + \bar{d} + 150 \mu\text{m}$, where w_{real} is the desired dimension after fabrication and w_{design} is the respective length introduced in the design scheme. The sign of \bar{d} is positive when designing outer structures (plugs) and negative for inner structures (sockets). Some examples of fabricated individual building blocks and a completely assembled CWI are shown in Fig. 2b.

3.4 Optical characterization

In all experiments, a fiber-coupled red laser (635 nm, 2.5 mW, Thorlabs, Inc.) connected to a FC/PC-SMA multimode fiber (Thorlabs, Inc.) with a core/cladding diameter of 200/230 μm and a numerical aperture NA of 0.22 was employed as the light source. A QE Pro 65000 photo-spectrometer (Ocean

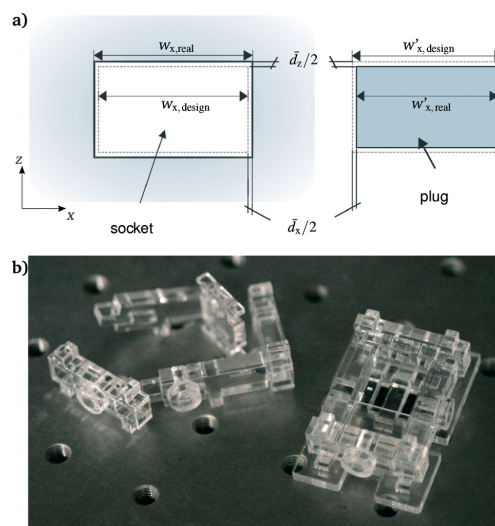


Fig. 2 a) Schematic illustration of the design schemes for the laser cutting of plugs and sockets and b) photograph of the laser-fabricated constituent parts and the fully assembled CWI.

Table 1 Characteristics of Epilog Mini 24

Working wavelength	10.62 μm
Maximum power	24 W
Maximum cutting speed	88.9 mm s ⁻¹
Resolution	1200 dpi max.
Precision of xy-positioning	$\pm 12.7 \mu\text{m}$

Optics) served as the detector. To obtain a 2D-mapping of the output plane, a pig-tailed 50/125 μm fiber was mounted on a motorized xz -stage (Micos VT80, Eschenbach, Germany) perpendicular to the edge of the PhLoC to scan the area around the WG end-facet with a step size of 10 μm . Movement and intensity acquisition were controlled by a LabVIEW script to obtain the complete mapping of the optical output plane (compare Fig. S5, ESI†). The intensity at 635 nm was collected at each point for a constant input power of 0.25 mW and with an integration time of 25 ms. SMA–SMA multimode fiber-optics (Thorlabs, Inc.) with core/cladding diameters of 50/125 μm , 105/125 μm and 200/230 μm and a numerical aperture NA of 0.22 were used to evaluate the plug-optics individually and their function as chip-to-world interfaces.

3.5 Simulations

Ray-tracing simulations emulating the experimental conditions were performed using TracePro (Lambda Research) for comparison. To that effect, 8×10^5 rays with a wavelength of 635 nm were traced through a 3D model of the PhLoC from a perfectly aligned, 2 m long input fiber-optics with a NA of 0.22. The waveguide's modal profile was examined in the form of an irradiance map on the output plane at 200 μm distance from the edge of the PhLoC.

4 Results and discussion

4.1 Evaluation of plug-optics

In order to assess the reproducibility and performance of the proposed plug-optics connectors, three sets of plug-optics were fabricated and assembled in all possible combinations to form a three-slot fiber-to-fiber connector. To that end, they were interlocked with and held together by auxiliary bottom and top pieces (detailed schemes can be found in the ESI†, Fig. S2). Fiber-to-fiber coupling was evaluated by averaging the coupled intensity over the three combinations and the resulting plug-optics triplets. For constant input intensity, the average output intensity was recorded as a function of the size of the output fiber-optics. The results compared to those of a commercial two-slot fiber-connector are presented in Fig. 3. The statistical evaluation shows that there are no significant differences between the coupled intensities obtained using either of the connectors. The plug-optics connectors though show more variation as a result of low-cost fabrication and assembly. This variation becomes more important the more similar the diameters of the input and output fiber-optics are.

4.2 Plug and measure

From the evaluation of the plug-optics coupler, it would seem that size mismatch between the emitting and receiving ends ensures reliable and reproducible, if inefficient, coupling. Robust fiber-to-chip coupling should therefore be viable using the proposed CWI in the case of sufficient size mismatch between on-chip photonics and fiber-optics. As another conse-

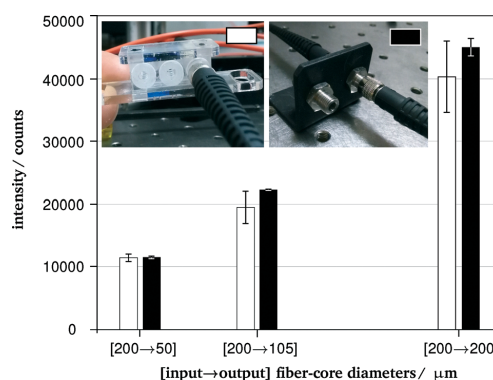


Fig. 3 Evaluation of the 'plug optics' concept. The average intensities coupled from fiber-optics to fiber-optics using plug-optics and a two-slot commercial fiber-connector are compared.

quence, an important fraction of the incoming light would not be coupled to the WG, but propagate as stray light through the structure and may thus to some extent contribute as noise to the optical readout.

4.2.1 Signal-to-noise ratio (SNR). In this context, as a next step, we assessed the contribution of stray light to the output signal on the basis of the previously described PhLoC. An intensity mapping of the output plane in an area A of $500 \times 500 \mu\text{m}^2$ around the center of the WG and at a distance of 200 μm from the edge of the PhLoC was used to assess the signal-to-noise ratio (SNR). The simulated and experimental results are presented in Fig. 4.

Fig. 4a shows the light propagation through the model PhLoC according to the ray-tracing simulation conducted with TracePro. Due to inefficient coupling (insertion losses of 15.4 dB are to be expected according to the simulation), a large portion of incoming rays result in stray light. Yet, no stray light reaches the output plane: the irradiance map obtained from the rays incident on A shows no measurable incident radiation apart from a localized and sharply peaked intensity profile corresponding to the multi-modal SU-8 waveguide with a $90 \times 6 \mu\text{m}^2$ cross-section. As a result of the high numerical aperture of the WG, an extensive expansion of this profile with the distance from the end-facet of the waveguide could be expected. This is reflected in the profile's dimensions of roughly 200 μm in the x -direction and 70 μm in the z -direction found in the irradiance map.

Fig. 4b shows the experimental fiber-to-chip coupling using the proposed CWI and 2D-mapping of the resulting output profile. In the photograph, the end-facet of the WG can be identified as a confined bright spot in the center of the small square, which corresponds to the scanning area A . The picture demonstrates that light is coupled successfully *via* the plug-optics to the thin SU-8 waveguide and guided through the bend to the output. The mapping result shows a localized and sharply peaked region of high intensity (signal S) with a maximum peak intensity of $S_{\text{max}} = 35\,900$ counts \equiv

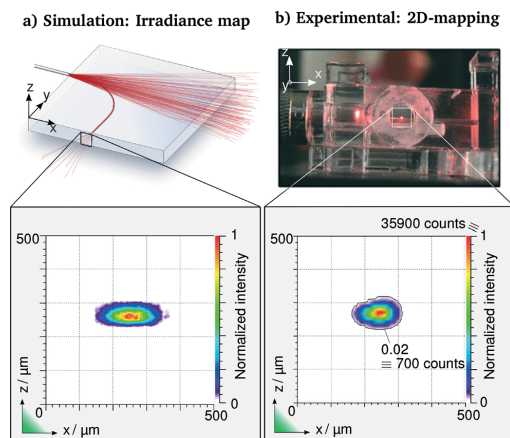


Fig. 4 a) Ray-tracing simulation (using TracePro, Lambda Research) of a 90° bent SU-8 waveguide (cross-section: $6 \times 90 \mu\text{m}^2$) on a glass substrate. 8×10^5 rays with a wavelength of 635 nm are traced through the model via a 2 m long fiber-optics (200/230 μm , NA = 0.22) aligned with the waveguide. An irradiance map shows the intensity profile of the waveguide output on the x - z plane at 200 μm distance from the waveguide's end-facet. b) $500 \times 500 \mu\text{m}^2$ 2D-mapping around the WG output obtained by using pig-tailed 50/125 μm fiber-optics mounted on a motorized stage and the resulting 3D profile.

1 corresponding to the WG output. It is worth noting that the experimental output profile is more localized than the simulated one. This can be attributed to the low numerical aperture of the scanning fiber-optics. While in the simulation all rays incident on A contribute to the profile, radiation at large angles is discarded in the experiment. The contour line in the 2D profile marks the threshold between what can be considered the waveguide output and background noise N and defines the profile with an effective width of $\approx 160 \mu\text{m}$ in the x -dimension. In the scanned area outside the contour line, the recollected intensity does not exceed a maximum of $N_{\text{max}} = 700 \text{ counts} \equiv 0.02$. We therefore assume that, as a consequence of the introduced WG bend, stray light indeed does not contribute as noise to the readout on the output plane. Hence, in the case of optimal alignment of the receiving 50/125 μm fiber-optics with the waveguide output and a relatively low input power of 0.25 mW, we achieve a signal-to-noise ratio of $\text{SNR} = S_{\text{max}}/N_{\text{max}} = 50$.

The sharpness of the intensity profile indicates that, depending on the diameter of the fiber-optics employed as output, small deviations in alignment and positioning may result in significant variations of the readout. On the other hand, insight into the measured SNR fiber-optics with large (up to 500 μm) core diameters could be used for the readout in order to provide sufficient alignment margins and achieve maximum output without significant noise contribution. In the following section, we explore the robustness and repeatability of the readout provided by the proposed CWI applying different alignment margins.

4.2.2 Robustness and repeatability of measurements. The completely assembled CWI, with PhLoC as well as fiber-optics input and output plugged in, is shown in Fig. 5a. In this configuration, we studied the influence of fabrication precision, assembly/disassembly and repeated positioning and alignment of PhLoC and fiber-optics on the output signal. The input unit (compare Fig. 1c) was fabricated twice and, exchanging this part between each measurement and plugging in the PhLoC anew, the output intensity was collected subsequently by different output fiber-optics. Varying the diameter of the output fiber-optics results in different overlap situations of fiber-optics and the intensity profile originating from the WG. As apparent from Fig. 5a, misalignment may produce strong variations of signal intensity using a 50/125 μm fiber as output, while the intensity may well be invariable to small misalignments using a 200/230 μm fiber.

As shown in Fig. 5b, the experimental value obtained using the 50/125 μm fiber-optics indeed shows significant variation. Using the 105/125 μm fiber-optics, this variation is

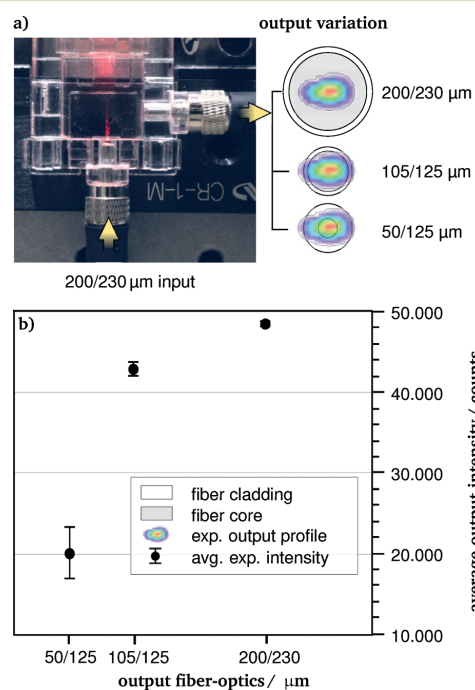


Fig. 5 a) Plug and measure. Photograph of CWI with plugged PhLoC and fiber-optics showing fiber connection and light coupling to and from the PhLoC. For different output fiber-optics, the relative dimensions of the experimental output intensity profile at 200 μm distance from the WG and the fiber-optics cross-sections are shown schematically. b) Measured intensities corresponding to different fiber-optics configurations. The error bars correspond to experimental intensity variations of 7.5% using 50/125 μm , 3.3% using 105/125 μm and 0.6% using 200/230 μm fiber-optics as output.

greatly reduced and, using the 200/230 μm fiber-optics, no significant signal variation is obtained.

These results are in line with the previous findings and show that the combined alignment variations induced by fabrication precision (compare Table 1), repeated assembly/disassembly and plugging in and out of the PhLoC are fully compensated by the alignment margins of $\pm 20\ \mu\text{m}$ provided by using 200/230 μm fiber-optics for input and output.

Together with the obtained SNR = 50, this validates the proposed methodology of fabrication and assembly as a robust and cheap solution for PhLoC-to-world connections which could be employed beneficially in a series of already developed PhLoCs with different approaches integrating, for instance, optical spectroscopy,^{31,33} flow cytometry^{34–38} or photonic whispering gallery mode (WGM) structures for label-free molecular detection^{39,40} in microfluidic systems.

5 Conclusions

We have presented a cheap, robust and easy-to-use chip-to-world interface for photonic lab-on-a-chip devices (PhLoCs). Comparing the proposed plug-optics SMA fiber connections by themselves to a commercial fiber-to-fiber connector, we found that the performance was not significantly different. This standardization gives great versatility to the interface, providing a direct link between PhLoCs and a wide range of light sources and photo-detectors.

Experimental evaluation of the fully assembled CWI showed that the introduction of bends in the photonic structure allowed stray-light artefacts to be efficiently discarded and a clean signal with a good signal-to-noise ratio (SNR = 50) to be obtained. In this optimized configuration, it could be shown that alignment margins of ± 20 suffice to fully compensate for misalignments induced by fabrication or assembly. Even through different cycles of fabrication and assembly as well as plugging in and out of the PhLoC, coupling to SU-8 multimode waveguides as thin as 6 μm has been demonstrated without significant signal variation.

The fact that PhLoCs can be easily plugged in and out by a user without a special skill-set while obtaining full functionality is a big step forward in terms of user-friendliness and potentially brings PhLoCs one step closer towards practical applications.

Acknowledgements

The research leading to these results has been partly funded by the European Union's Seventh Framework Programme (FP7/2007–2013) under grant agreement no. 317916. X. Muñoz-Berbel acknowledges the Spanish Ministry of Economy and Competitiveness for the Ramon y Cajal grant. P. Giménez-Gómez is grateful to MINECO, Spain for the financial support through a research studentship of the FPI Program.

References

- 1 D. J. Beebe, G. A. Mensing and G. M. Walker, *Annu. Rev. Biomed. Eng.*, 2002, **4**, 261–286.
- 2 C. Haber, *Lab Chip*, 2006, **6**, 1118–1121.
- 3 D. Mark, S. Haeberle, G. Roth, F. von Stetten and R. Zengerle, *Chem. Soc. Rev.*, 2010, **39**, 1153–1182.
- 4 D. J. Laser and J. G. Santiago, *J. Micromech. Microeng.*, 2004, **14**, R35–R64.
- 5 P. Woias, *Sens. Actuators, B*, 2005, **105**, 28–38.
- 6 K. W. Oh and C. H. Ahn, *J. Micromech. Microeng.*, 2006, **16**, R13–R39.
- 7 V. Hessel, H. Löwe and F. Schönfeld, *Chem. Eng. Sci.*, 2005, **60**, 2479–2501.
- 8 N.-T. Nguyen and Z. Wu, *J. Micromech. Microeng.*, 2005, **15**, R1–R16.
- 9 C. Y. Lee, C. L. Chang, Y. N. Wang and L. M. Fu, *Int. J. Mol. Sci.*, 2011, **12**, 3263–3287.
- 10 D. G. Rackus, M. H. Shamsi and A. R. Wheeler, *Chem. Soc. Rev.*, 2015, **44**, 5320–5340.
- 11 B. Kuswandi, Nuriman, J. Huskens and W. Verboom, *Anal. Chim. Acta*, 2007, **601**, 141–155.
- 12 K. B. Mogensen and J. P. Kutter, *Electrophoresis*, 2009, **30**, 92–100.
- 13 M. C. Estevez, M. Alvarez and L. M. Lechuga, *Laser Photonics Rev.*, 2012, **6**, 463–487.
- 14 G. M. Whitesides, *Nature*, 2006, **442**, 368–373.
- 15 N. Pires, T. Dong, U. Hanke and N. Hoivik, *Sensors*, 2014, **14**, 15458–15479.
- 16 E. K. Sackmann, A. L. Fulton and D. J. Beebe, *Nature*, 2014, **507**, 181–189.
- 17 C. D. Chin, V. Linder and S. K. Sia, *Lab Chip*, 2012, **12**, 2118.
- 18 L. R. Volpatti and A. K. Yetisen, *Trends Biotechnol.*, 2014, **32**, 347–350.
- 19 C. K. Fredrickson and Z. H. Fan, *Lab Chip*, 2004, **4**, 526–533.
- 20 M. I. Mohammed, S. Haswell and I. Gibson, *Procedia Technol.*, 2015, **20**, 54–59.
- 21 E. Wilhelm, C. Neumann, T. Düttenhofer, L. Pires and B. E. Rapp, *Lab Chip*, 2013, **13**, 4343–4351.
- 22 D. van Swaay, J.-P. Mächler, C. Stanley and A. DeMello, *Lab Chip*, 2014, **14**, 178–181.
- 23 Y. Temiz, R. D. Lovchik, G. V. Kaigala and E. Delamarche, *Microelectron. Eng.*, 2015, **132**, 156–175.
- 24 N. Blow, *Nat. Methods*, 2007, **4**, 665–670.
- 25 H. Becker, *Lab Chip*, 2009, **9**, 2119–2122.
- 26 R. Horvath, H. C. Pedersen, N. Skivesen, C. Svanberg and N. B. Larsen, *J. Micromech. Microeng.*, 2005, **15**, 1260–1264.
- 27 S. Balslev, A. M. Jorgensen, B. Bilenberg, K. B. Mogensen, D. Snakenborg, O. Geschke, J. P. Kutter and A. Kristensen, *Lab Chip*, 2006, **6**, 213–217.
- 28 X. Wang, M. Amatongchai, D. Nacapricha, O. Hofmann, J. C. de Mello, D. D. C. Bradley and A. J. de Mello, *Sens. Actuators, B*, 2009, **140**, 643–648.
- 29 A. Llobera, J. Juvert, A. González-Fernández, B. Ibarlucea, E. Carregal-Romero, S. Büttgenbach and C. Fernández-Sánchez, *Light: Sci. Appl.*, 2015, **4**, e271.

- 30 G. de Cesare, A. Nascetti, R. Scipinotti, A. Zahra and D. Caputo, *Sens. Biosensing Res.*, 2015, 3, 53–58.
- 31 I. Rodríguez-Ruiz, T. N. Ackermann, X. Muñoz-Berbel and A. Llobera, *Anal. Chem.*, 2016, 88(13), 6630–6637.
- 32 S. Prakash and S. Kumar, *Int. J. Precis. Eng. Man.*, 2015, 16, 361–366.
- 33 A. Prabhakar and S. Mukherji, *International Conference on Systems in Medicine and Biology*, ICSMB 2010 - Proceedings, 2010, pp. 67–70.
- 34 B. R. Watts, Z. Zhang, C.-Q. Xu, X. Cao and M. Lin, *Biomed. Opt. Express*, 2012, 3, 2784–2793.
- 35 P. Fei, Z. Chen, Y. Men, A. Li, Y. Shen and Y. Huang, *Lab Chip*, 2012, 12, 3700–3706.
- 36 J. Godin, C. H. Chen, S. H. Cho, W. Qiao, F. Tsai and Y. H. Lo, *J. Biophotonics*, 2008, 1, 355–376.
- 37 J. Godin, V. Lien and Y. H. Lo, *Appl. Phys. Lett.*, 2006, 89, 2006–2008.
- 38 Z. Wang, J. El-Ali, M. Englund, T. Gotsaed, I. R. Perch-Nielsen, K. B. Mogensen, D. Snakenborg, J. P. Kutter and A. Wolff, *Lab Chip*, 2004, 4, 372–377.
- 39 T. Wienhold, S. Kraemmer, A. Bacher, H. Kalt, C. Koos, S. Koeber and T. Mappes, *Opt. Express*, 2015, 23, 1025.
- 40 U. Bog, F. Brinkmann, S. F. Wondimu, T. Wienhold, S. Kraemmer, C. Koos, H. Kalt, M. Hirtz, H. Fuchs, S. Koeber and T. Mappes, *Adv. Sci.*, 2015, 1–6.

A.1.4

Electronic Supplementary Information

Plug and Measure - a chip-to-world interface for photonic lab-on-a-chip applications[†]

Tobias Nils Ackermann,^{*,‡} Pablo Giménez-Gómez,^{*} Xavier Muñoz-Berbel^{*} and Andreu Llobera^{*}

Plug-optics and CWI: Schemes

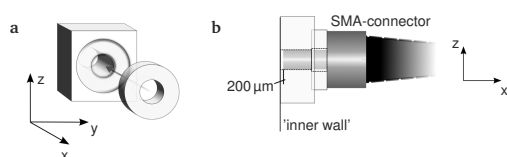


Fig. S1 **a** Detail of plug-optics assembly. To fabricate the plug-optics connector, a cylindrical socket with a design-diameter of 3 mm is laser-cut into 5 mm thick PMMA applying the optimized conditions $P = 100$, $S = 5$ and $F = 5000$ at 1200 dpi using the Epilog Mini 24 laser writer. Subsequently, the thickness of the block is reduced in a concentric circular area by laser engraving applying 'raster' conditions of $P = 35$, $S = 12$ and $F = 5000$ at 1200 dpi. A 3 mm thick PMMA disk comprising a cylindrical socket with 3.5 mm design-diameter cut applying $P = 100$, $S = 5$ and $F = 5000$ and equally reduced in thickness by laser-engraving. The disk is glued into the pre-structured area on the 5 mm thick PMMA. **b** A SMA fiber-connector plugged into the described unit is firmly clamped, leaving the end-facet at a distance of approximately 200 μm from the 'inner wall'.

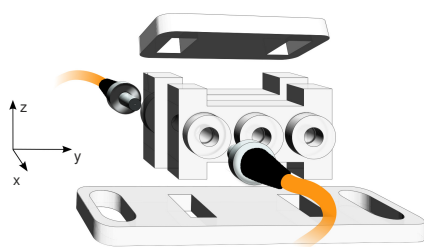


Fig. S2 Schematic detail of triple plug-optics fiber-connector.

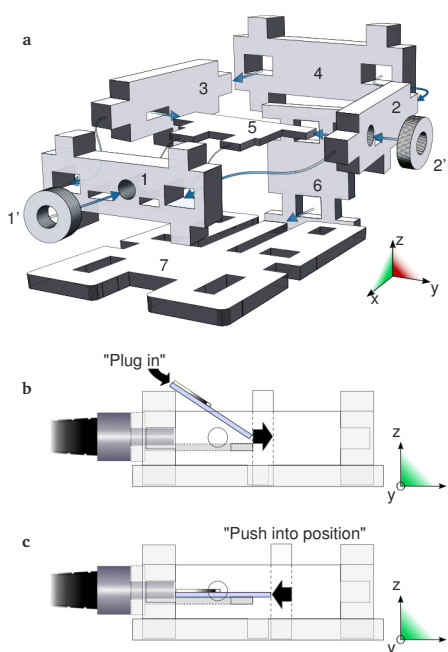


Fig. S3 **a** Model of the individual building blocks and their assembly. 1, 2: Primary building blocks defining the input and output plane comprising sockets for SMA-connectors and platform 5; 1', 2': Spacer disks adjusting the distance from fiber-optics to edge of PhLoC; 3: Side-wall comprising socket to sustain 5; 4: Back-piece completing the outer frame; Blocks 1 – 4 are anchored in the base to assure right angles and provide additional stability; 5: Platform to sustain the PhLoC at the corresponding height relative to the fiber-optics; 6: Base of CWI comprising track to guide movement of unit 6; 6: Mobile unit anchored to tracks in the base in order to be moved back and forth clamping the PhLoC in place or releasing it. **b-c** Schematic illustration of how the PhLoC is plugged into the CWI and pushed in position (aligned with the SMA fiber-connector)

^{*} Institut de microelectrónica (IMB-CNM), Campus UAB, E-08193 Cerdanyola del Val·lès, Spain. Fax: (+34) 93 580 1496; Tel: (+34) 93 594 7700

[‡] corresponding Author; Tel: (+34) 93 594 7700 (ext. 2431); E-mail: tobias.ackermann@imb-cnm.csic.es

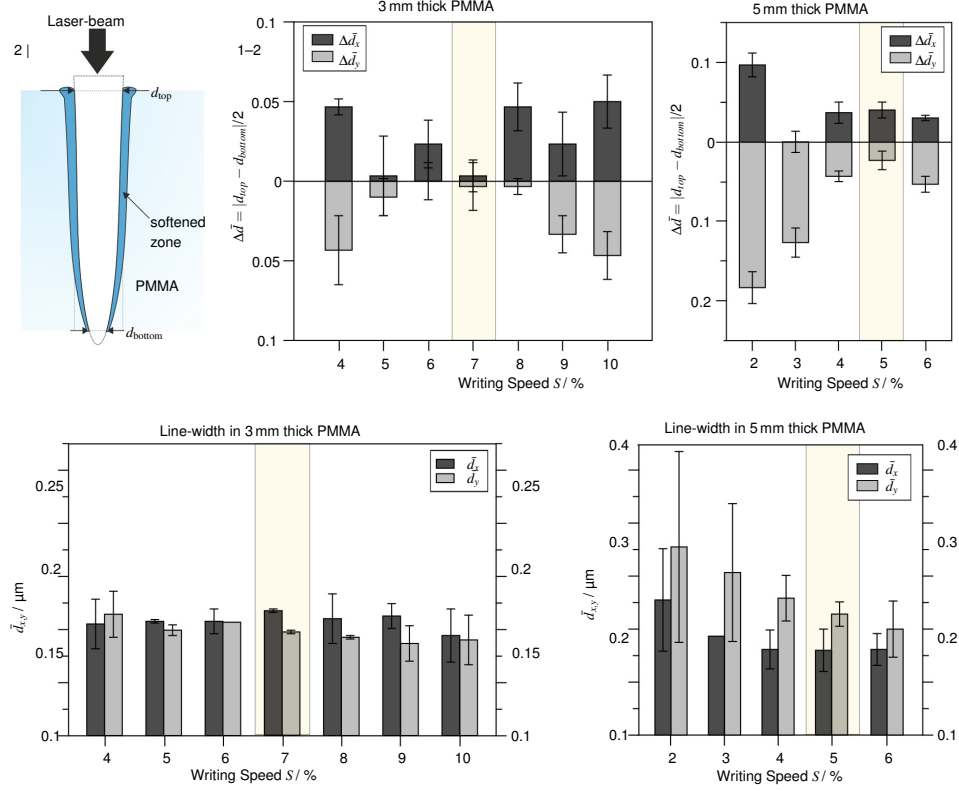


Fig. S4 CO₂ laser fabrication Differences of d_{top} and d_{bottom} for a series of cutting speeds in 5 mm and 3 mm thick PMMA respectively, keeping $P = 100$ and $F = 5000$ constant. The condition in which this difference was smallest and less dependent on the writing direction is highlighted and was used to set the design dimensions. The schematic illustration of the cutting profile in the upper left is based on findings of Prakash et al.⁷ and own observations.

Photo-lithography for waveguide fabrication

First, a borosilicate (Pyrex®) wafer was exposed to O₂-plasma during 18 seconds at 480 W to activate the surface. SU-8 2005 was spincoated at 3000 rpm and submitted to a pre-bake for 20 min at 95 °C after an initial temperature ramp from 65 to 95 °C during 15 min. Waveguides were defined by exposing the pre-baked SU-8 through a Film Mask ordered from JD Photo Data in a KS A6 mask aligner (Karl Süss) with a dose of 330 mJ/cm³. The exposed structures were post-exposure baked for 10 min at 95 °C with ramp as before.

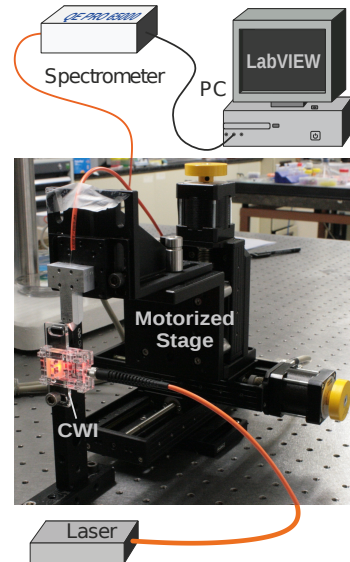


Fig. S5 Setup Experimental setup used for the 2D-mapping of the WG output.

A.1.5


Photonic Lab-on-a-Chip: Integration of Optical Spectroscopy in Microfluidic Systems

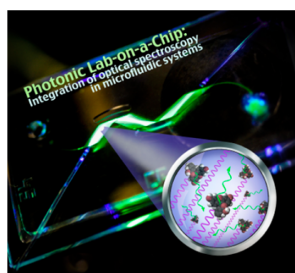
The integration of micro-optical elements with microfluidics leads to the highly promising photonic lab-on-a-chip analytical systems (PhLoCs). In this work, we re-examine the main principles which are underneath the on-chip spectrophotometric detection, approaching the PhLoC concept to a nonexpert audience.

Isaac Rodríguez-Ruiz,^{†,‡,§} Tobias N. Ackermann,^{†,§} Xavier Muñoz-Berbel,[†] and Andreu Llobera^{*,†}

[†]Institut de Microelectrònica de Barcelona—CNM/CSIC Campus UAB, 08193 Cerdanyola del Vallès, Barcelona, Spain

[‡]CEA, DEN, DTEC, SGCS, F-30207 Bagnols-sur-Cèze, France

 Supporting Information



With the aim to miniaturize and integrate most of the required steps of an analytical assay, lab-on-a-chip (LoC) technology has gained significant weight in the last 2 decades. In this context, miniaturization allows not only a decrease of the required analysis time, sample volume, and reagent consumption but also results in an enhancement of the sensitivity and the possibility to parallelize the analysis without dramatically increasing both the complexity and the system footprint. As a result, from the early micro total analysis system (μ TAS) concept,¹ nowadays it is possible to find in the literature a myriad of extremely sophisticated LoC for applications such as drug discovery and development,² genomics,³ clinical diagnosis,⁴ or cellomics.⁵ In most of these examples, a superior performance as compared to bulk analytical setups in terms of sensitivity to a specific analyte is obtained.

However, most of the LoCs still rely on external and complex instrumentation for analyte detection and quantification. As a result, they still fail to be more widely established alongside standardized laboratory protocols and techniques and, more importantly, in real applications outside controlled laboratory environment. The integration of transducers able to transform a biological/chemical reaction into a quantifiable signal will represent a turning point of the LoC paradigm. Steps toward this issue have been taken and different transduction mechanisms have already been integrated in a LoC, such as electrochemical,⁶ magnetic,⁷ or optics/phonics.⁸ Among them, optical transducers have demonstrated to be one of the

most sensitive and selective analytical detection methods,⁹ while providing the unmatched property of prevailing sample sterility due to its noncontact measurement principle.

Light manipulation and confinement in liquid materials, and specially in microfluidic environments, has generally been called optofluidics.¹⁰ In one branch of optofluidics, fluids play an active, key role in handling, and directing the propagation of light in the microsystem (however, this is a step further in complexity). A major advantage here is the atom-sized roughness between two immiscible fluids with different refractive index (RI), resulting in optically flat surfaces. Not surprisingly, this concept has been exploited in liquid–liquid waveguides¹² and in optofluidic routers.¹³

Alternatively, the synergistic combination of photonic integrated circuits (PICs) with LoC gives rise to the photonic lab-on-a-chip (PhLoC) concept,¹¹ where the advantages of both research fields are merged. Here, the main function of microfluidics is the manipulation and transport of the analytes, while the PICs transduce the (bio)chemical signal arising from the analytes in situ to a quantifiable signal.

In this work we aim to provide an introduction to the integration of optical spectroscopy with LoC by means of fundamental optical elements, i.e., microlenses and mirrors. We describe the nuts and bolts of the conception of such PhLoC systems based on two main keystones: (i) the selection of the appropriate detection mechanism, i.e., colorimetry, fluorimetry, and/or dispersion/scattering, and (ii) the design of the PhLoC, considering both the optical properties of the materials and the geometry of the optical elements. Finally, the application of this paradigm is demonstrated through some examples showing different and low cost approaches to solve real analytical problems.

■ BASIC PRINCIPLES: SPECTROPHOTOMETRIC MEASUREMENTS ON CHIP

Within the previously mentioned spectrophotometric techniques, both colorimetry and scattering assays can be measured longitudinally through the bulk of the sample. The propagation through the sample results in an attenuation of the light, which

Published: May 6, 2016



ACS Publications

© 2016 American Chemical Society

6630

DOI: 10.1021/acs.analchem.6b00377
Anal. Chem. 2016, 88, 6630–6637

Analytical Chemistry

Feature

is proportional to the optical path length l (cm^{-1}) and the analyte concentration c (M), and is described by the Beer–Lambert law:¹⁴

$$A(\lambda) = -\log_{10}\left(\frac{I}{I_0}\right) = \varepsilon(\lambda)cl \quad (1)$$

where I_0 is the reference intensity measured through l in absence of analyte (e.g., only solvent), I is the intensity measured through the same optical path in presence of analyte, and ε is the molar attenuation coefficient of the analyte ($\text{M}^{-1}\text{cm}^{-1}$), which varies as a function of the wavelength. Note that in most cases the attenuation of the sample (extendedly called absorbance A with absorbance units A.U.) is due to absorption as well as scattering. Scattering events do however not add linearly to extinction. Depending on the scattering anisotropy (g , dimensionless) of the analyte, a portion of light is scattered in the forward direction ($g = 1$ implies purely forward, $g = 0$ backward scattering) and still detected in the longitudinal direction.

It should also be mentioned that not only the analyte itself contributes to attenuation of the incident beam. Reflections at interfaces (depending on the contrast of refractive index at the interface) as well as the proper solvent may also cause attenuation. It is thus crucial for the accuracy of the measurement that I_0 (which corresponds to 100% transmittance) is measured with the same optical system and same interface conditions as used to measure I .

Experimentally, it is accepted that eq 1 presents a linear behavior for absorbance values within 0 and 1 A.U. The deviation from the linearity postulated by the Beer–Lambert law is commonly observed for high analyte concentrations for a fixed l value, e.g., due to a change in refractive index of the solution or aggregate formation, which is not considered in the Beer–Lambert law derivation. The sensitivity of such measurements is given by the slope in the linear range. It is reasonable to consider that the shorter the optical path, the lower the sensitivity, though the contrary (i.e., the longer the optical path, the higher sensitivity) does not apply *ad infinitum*, as there are other factors working against. First, it must be considered that light sources are inherently divergent and, unless proper 3D optical elements are included in the microsystem, the optical losses increase with the optical path length. As a consequence, the signal-to-noise ratio (SNR) quickly decreases for large optical paths. Additionally, we also need to satisfy the compactness constraint required for LoC applications.

In contrast to colorimetry and scattering assays as described above, fluorimetry does not rely on the quantification of attenuation. Fluorescence is the transition from an absorption induced excited electronic state to a state with a lower energy by emission of a photon. As such it is proportional to absorption, but the emission occurs spontaneously in 4π steradians at a ratio of emitted versus absorbed photons called the quantum yield Φ . This homogeneous light emission allows multiplexing excitation and emission wavelengths when the detector is positioned 90° from the light source. In that way the fluorescence emission intensity can be decoupled from the excitation radiation, thus improving the SNR for the detection of light emitted by the analyte. It should however be kept in mind here that only a fraction of light emitted with the appropriate solid angle can be detected, unless integrating spheres are used. Under the assumption that attenuation is here

solely due to absorption, the fluorescence intensity measured at wavelength λ_F can then be written as

$$I_F \propto k\Phi(1 - (10^{-A})) = k\Phi I_0(1 - (10^{-\varepsilon cl})) \quad (2)$$

where the proportionality factor k depends on several parameters, in particular on the optical configuration for observation (i.e., the solid angle through which the instrument collects fluorescence) and ε refers strictly to absorption. For low analyte concentrations (and accordingly low absorption along the optical path), eq 2 can be approximated to¹⁵

$$F = kI_0\Phi(\varepsilon cl) \quad (3)$$

Consequently, in order to perform classical spectrophotometric analyses on-chip with enhanced sensitivity, it is important to attune the PhLoC design to the specific application and to optimize crucial parameters. In particular, the use of micro-optic elements for light collimation or focusing can be very useful for boosting light coupling/decoupling efficiency and accuracy as well as optimizing light-sample interaction in optofluidic systems.

Micro-Optics Design and Fabrication. The design of micro-optic elements still complies with the basic optics laws as long as the diffraction limit is not reached. As such, the following assumptions must be considered.

From a practical point of view, one of the simplest ways to couple light to/from a PhLoC is by way of pigtailed fiber optics, as these represent a standardized link to a wide range of light sources as well as photodetectors and photospectrometers. Thus, if the micro-optic elements are designed in accordance to the fiber optics parameters (numerical aperture and core diameter mainly), they can be readily included in the PhLoC as a basic element independent of the particular application.

Concerning the concrete optical design it should be mentioned that a light beam is bent at an interface between two materials according to the well-known Snell's law,¹⁶

$$n_1 \sin(\theta_1) = n_2 \sin(\theta_2) \quad (4)$$

where n_1 and n_2 are the respective refractive indices of the adjacent materials and θ_1 and θ_2 are, respectively, the incident angle in the first material (with respect to the surface normal) and the new angle after passing the interface.

Equation 4 provides the basic tool to understand beam propagation at the interface between two materials by knowing the incidence angle and the involved refractive indices. Another implication of eq 4 is that there exists a critical angle of incidence

$$\theta_c = \sin^{-1}\left(\frac{n_1}{n_2}\right) \quad (5)$$

above which light is totally internally reflected (TIR condition). Accordingly, the contrast in refractive index at an interphase between adjacent materials can also be used to define mirrors, which act upon all rays fulfilling this condition.

A second well-known formula is the so-called lensmaker's equation¹⁶

$$\frac{1}{f} = (n_1 - 1) \left[\frac{1}{R_1} - \frac{1}{R_2} + \frac{(n_1 - 1)d}{R_1 R_2} \right] \quad (6)$$

where f is the focal length, R_1 and R_2 are the radius of curvature, and d is the thickness of the lens (which can be considered zero for thin lenses). Thus, by carefully combining curved interfaces

Analytical Chemistry

Feature

(as shown in Figure 1a) with known refractive indices, light shape, and propagation can be modified so as to match with the

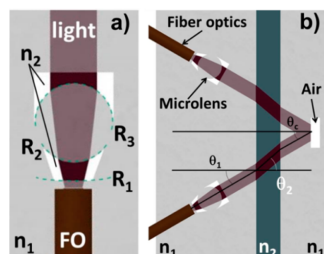


Figure 1. Schematic representations of (a) the conception of a collimating set of lenses with curvature radii R_{1-3} optimized for the use with fiber optics of a defined numerical aperture and (b) the interaction of different micro-optic elements to enhance light–sample interaction: A first set of microlenses collimates the incoming beam, which then travels across the microchannel filled with analyte, is reflected back across the channel and finally focused on the output fiber optics by the second inversely operated set of microlenses. Figure adapted from ref 17 and reproduced with permission of Nature Protocols. Copyright 2011 Nature Publishing Group.

specific requirements of a given PhLoC application. It is important here to say that what is required for managing the light flow is an interface between two materials with different refractive indices. The most common (and sometimes overlooked) material is air, which can indeed be used as an active material for defining any kind of micro-optical element.

Optofluidic System Design. Figure 1b schematically shows one example of how these optical phenomena can be employed in a PhLoC, combining two sets of collimating microlenses, light-sample interaction, and a flat air mirror to double the optical path through the sample. Initially, the fiber optics is inserted in so-called self-alignment channels, which allow clamping the fiber optics at the required specific distance from the lens, typically the focal length, and perfectly aligned with the optical axis. Light arising from a pigtailed fiber optics is collimated by a first set of focusing cylindrical lenses (Figure 1a; the figure can be found in the Supporting Information). Specifically, the imprinted air structures of the microlenses comprise curved surfaces, whose curvature radii are chosen based on the refractive index contrast between air and the construction material. Thus, a major part of the incoming light can be directed along the intended axis and interact with the analyte in the microfluidic channel. The refraction of the beam at the interphase between construction material (n_1) and the analyte solution (n_2) according to eq 2 is also to be considered in the design for correct relative positioning. After crossing the channel, the collimated beam strikes a flat air pocket (air mirror) with an incident angle above θ_c and is consequently reflected back across the channel and focused onto the tip of an output fiber optics via a set of inversely operated microlenses. Given this working principle, it is shown that a set of geometric considerations such as radii of curvature and angles of incidence, based on the construction material at hand, allows one to construct micro-optical elements for precise and efficient light handling, suitable for the integration in PhLoCs. Another important issue is that the integration of such micro-optical

elements does not increase the technological complexity, since they can be implemented jointly with the microfluidics mask.

Fabrication. A fabrication technique especially suited to integrate such micro-optical elements in microfluidic systems is soft-lithography.¹⁷ The technique is well-established in the domain of μ TAS and is based on the direct transfer of planar structures with features in the micro- and nanoscale from prepatterned molds or stamps, so-called masters, into soft elastomeric materials with high transparency at UV–vis wavelengths. One of the most widely used materials fulfilling these requirements is polydimethylsiloxane (PDMS), a silicon-based organic polymer which is optically clear, cheap, and nontoxic. The replicas, made with PDMS or any other material, feature the negative of the patterns contained in the masters as imprints (air gaps) with well-defined geometry. In this way, PhLoC systems can be monolithically imprinted in a single step, assuring a perfect alignment of micro-optic and microfluidic elements by design. Moreover, the resulting alternation between air and construction material in the optical path provides with the required refractive index contrast and therefore efficient light beam modulation by the interphases.

■ APPLYING AND DEVELOPING THE BASIC CONCEPTS

Single and Multiple Internal Reflection. From eq 1 it becomes clear that PhLoCs working in absorbance should ideally have the longest possible optical path, so as to enhance its sensitivity. It must be kept in mind, however, that the microlenses fabricated with soft lithography are not spherical but cylindrical. As such, they do not have a focal point but rather a focal plane (light sheet). In other words, the beam broadening in the vertical direction is not corrected, thus decreasing the SNR. Still, with the help of the air mirrors it is possible to lengthen the optical path in a PhLoC without causing an important increase of the footprint. In that sense, the simplest configuration is based on the so-called single internal reflection (SIR) systems,¹⁸ which can be seen in Figure 2a. Light is coupled by means of a biconvex microlens to a hollow Abbe prism. With the help of a flat air mirror, light bounces with a 60° angle toward the second biconvex microlenses and is finally collected with the output fiber optics. Such SIR PhLoCs have been applied for measurements of fluorescein¹⁹ and methyloange,²⁰ for the detection of heavy metal ions²¹ or as an element of an optical-electrochemical tongue for the quality control of wine.²²

Furthermore, with the adequate enzymatic functionalization, the prisms have been transformed into biocatalytic sensing reactors where enzyme activity has been measured.²³ An overview of the different applications, each PhLoC configuration and their respective limit of detection (LoD) (using a k value of 3, ensuring a confidence level of 99.87%)²⁴ can be found in Table 1, together with other PhLoC applications and configurations. Sensitivity can be further enhanced by increasing the optical path, but at a cost of increasing the SIR system size. An alternative is to shift from single to multiple reflections. Air mirrors can be defined at both sides of a given microfluidic system and then, by means of TIR, make light follow a zigzag path. In addition, the shape of the air mirrors can be arbitrarily defined: in that sense, in Figure 2b, focusing air mirrors allow one to have focal planes inside the microfluidic system. Note that the use of focusing elements implies the necessity to adapt the channel length to the focal length. These kind of PhLoCs, called multiple internal reflection (MIR)

6632

DOI: 10.1021/acs.analchem.6b00377
Anal. Chem. 2016, 88, 6630–6637

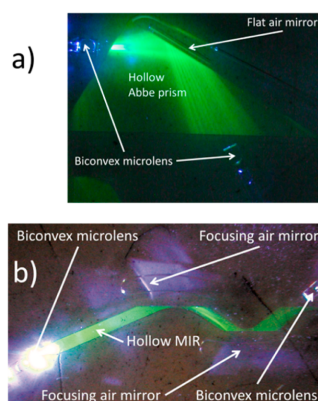


Figure 2. (a) SIR structure filled with buffer solution + 50 μM of fluorescein, where light reflection can be seen at the air mirror; (b) MIR structure filled with buffer solution + 10 μM of fluorescein, showing the zigzag path of the light inside the sensing region. Figures published in refs 11 and 18 and reproduced by permission of The Royal Society of Chemistry. Copyright 2007 and 2008, respectively.

systems, have demonstrated to have LoDs between 110 nM and 41 nM for fluorescein.¹¹ The potential of the MIR configuration is confirmed by the large number of applications and configuration where it has been used, e.g., in combination with electrochemical sensors (defining the Dual LoC) for L-lactate measurements²⁵ or for the classification of white grape juices with a multisensor (tongue) approach.²⁶ Additionally, they have been used as reactors for screening cell cultures, working in either scattering or scattering + absorption regimes,

both with LoDs close to 50 cells using monocytes and being able to distinguish between labeled (dead) and nonlabeled (alive) cells.^{17,27} A further step toward integration has been done by monolithically integrating a xerogel-based solid-state light emitter (SSLE) with a biofunctionalized MIR for detecting biocatalytic activity at very low substrate concentrations in the micromolar range.²⁸ A list of the different analytes measured with MIR structures can be found in Table 1.

Multiple Measurement Parallelization. Once a first degree of PhLoC complexity by the integration of microlenses for light beam collimation was achieved and taking advantage of MIR to elongate the interrogated optical path through the samples, a step forward in complexity is presented in the Multiple Path Photonic Lab-on-a-Chip (MPhIL).²⁹ This system, yet based on the same principles, allows the parallelization of multiple measurements within the same sample. MPhIL consists of a single serpentine channel describing 6 interconnected and different optical paths with lengths l varying from 0.05 to 1 cm (Figure 3a). In the case here described, optical interrogation channels (Figure 3a-1) comprise similar self-alignment elements and 2D microlenses to correct the beam broadening (Figure 1a-2). Air mirrors (Figure 3a-3) are located at both sides of the optical path with a 2-fold function: On the one hand, they form a waveguide-like structure by confining the light in the region where the microfluidics (and the analyte) is located, as it can be observed in the ray tracing simulation shown in Figure 3a-4. On the other hand, background noise and crosstalk is minimized, since such air mirrors allow one to block part of the light arising from either adjacent interrogation channels or from any other external source.

The MPhIL is based on multiple parallel absorbance measurements at constant concentration, performed on a single sample, while varying the optical path length. The so-

Table 1. Analytes, Configuration and LoD of the Different PhLoC Configurations Found in the Literature

Analyte	Configuration ^a	Type of measurement	LoD [μM]	Optical path [μm]	ref
Fluorescein	SIR	Fluorescence/absorbance	6	2387	19
Fluorescein	SIR	Fluorescence/absorbance	1.3–5.6	1790–3581	20
Fluorescein	SIR	Fluorescence/absorbance	1.03–1.08	2766, 3581	18
Methylorange	SIR	Absorbance	0.68–2.5	1790–3581	20
Methylorange	SIR	Absorbance	0.39	2766, 3581	18
pH	SIR	Absorbance	0.09–0.51	1790–3581	20
Wine	SIR (hybrid tongue)	Absorbance	-	3581	22
H ₂ O ₂	SIR+enzymatic functionalization (HRP)	Absorbance	0.12	3581	23
Hg ²⁺ /Pb ²⁺	SIR+ specific ligand	Absorbance	2.59/4.19	3581	21
Fluorescein	MIR	Fluorescence/absorbance	0.04–0.1	6357–14264	13
Monocytes	MIR	Absorbance/scattering	50 cells	8336	26, 17
L-Lactate	MIR+electrode	Absorbance	5	6357	24
Wine	MIR (tongue)	Absorbance	-	6357	25
Quinolone yellow/ H ₂ O ₂	MIR+SSLE	Absorbance	0.6/0.7	6357	27
Proteins	Multiple path LALC	UV-Absorbance	1.28/8.5	500–10000	29
H ₂ O ₂	^b LALC+enzymatic functionalization (HRP)	Absorbance	4.53	1000	25
Organic solvents	LALC	Absorbance	-	3000	2b
pH/Bacteria	LALC	Absorbance (180°)/ Fluorescence (90°)	0.32- 4.60 $\times 10^6$ cells	4200–5000	33
Crystal violet	MOPS	Absorbance (180°)/ Fluorescence (90°)	0.34 -	10500	36

^aAll the PhLoC configurations presented are fabricated in PDMS ($n = 1.41$ at $\lambda = 633$ nm), except for ref 2b, fabricated in SU-8 ($n = 1.58$ at $\lambda = 633$ nm). ^bLALC, micro-Lens-Assisted Light Collimation. Direct measurements performed with light input/output configured at 180°.

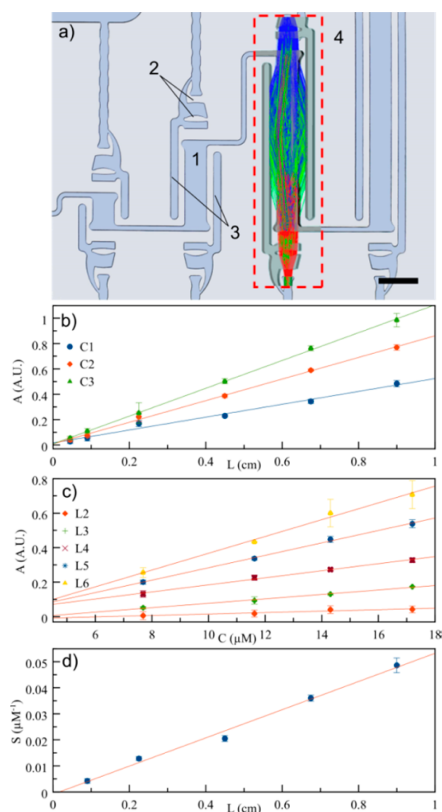


Figure 3. (a) Detail of a fabricated MPHIL. 2D microlenses and fiber optics channels can be seen at the ends of each optical path. (1) 2D microlenses; (2) air mirrors to prevent cross talking; (3) interrogation channel. Scale bar = 1 mm; (4) overlapped screenshot of a ray tracing simulation across one MPHIL OP, illustrating the performance of the included micro-optical elements (air mirrors and microlenses). (b) Plot of the absorbance measurements performed in the MPHIL as a function of different glucose isomerase protein concentrations for each MPHIL optical path. (c) Plot of the analytical sensitivity, S , as a function of optical path length. From the linear regression analysis of this plot, it is possible to calculate a limit path length of $L = (9.42 \pm 0.29) \times 10^{-2}$ cm. (d) Plots of the absorbance measurements performed with 3 different concentrations for dihydropyrimidinase from *S. meliloti* CECT41 protein, as a function of the optical path length (L): $C_1 = (8.37 \pm 0.03) \mu\text{M}$, $C_2 = (14.03 \pm 0.09) \mu\text{M}$, $C_3 = (18.0 \pm 0.1) \mu\text{M}$. Data adapted from ref 29 and reproduced by permission of The Royal Society of Chemistry. Copyright 2015.

called multiple path PhLoC configuration presents a series of advantages: it allows an increase in the linearity range relating concentration and absorbance in accordance to the Beer–Lambert law, as the measurements performed at shorter l values are transduced in a decrease of the absorbance signal (1). Additionally, analyte concentration or molar absorptivity can be obtained with a single injection step, as opposite to the standard calibration protocol, which requires a series of measurements at different concentrations. Figure 3b shows

absorbance experiments at $\lambda = 280$ nm, performed at 3 different concentrations for dihydropyrimidinase from *Sinorhizobium meliloti* CECT41 protein as a function of l , displaying the linear relation between both values, in agreement with eq 1. Protein concentrations were selected to present an absorbance below 1 A.U. (at $\lambda = 280$ nm) in the largest optical path of the MPHIL, allowing the parallel use of the 6 different optical paths for the measurements. R^2 coefficients calculated from the least-squares linear fitting of the data showed a good correlation degree ($R^2 > 0.98$) for all the measured concentrations.²⁹

Aside, the LoD for each optical path was also calculated. Using the above-mentioned analytical definition of LoD,²⁴ it is also possible to determine a limit value for the optical path lengths, allowing this to dynamically determine the optimal l values as a function of the analyte of interest. Calculations for this purpose were performed using another protein, glucose isomerase, as a model for the determination. Absorbance measurements as a function of different protein concentrations for each optical path are plotted in Figure 3c with their respective fittings, also displaying a good correlation. LoD values between $(1.28 \pm 0.04) \mu\text{M}$ and $(8.5 \pm 1.8) \mu\text{M}$, respectively, for the largest and shortest l are obtained for the model protein. Extracting the analytical sensitivity (S) from this plot (the slope of each linear fitting) and representing it as a function of the optical path (Figure 3d) we can determine a limit path length by means of another linear fitting analysis, obtaining a value of $L = (9.9 \pm 0.5) \times 10^{-2}$ cm. This limit path length value will correspond to the minimum l which would provide a measurable absorbance signal for the range of the studied analyte concentrations.

It is worth noting that the MPHIL can also be implemented and used as a multispectral detection component in more complex lab-on-a-chip systems, where the different multiple paths would permit both detection and quantification of the target analytes. Besides, the system is able to operate in the continuous flow regime, making it a good candidate to be used as a detection system for continuous sensing applications.

■ TOWARD ADVANCED SYSTEM INTEGRATION AND CONFIGURATION

Biophotonic Lab-on-a-Chip. One of the areas where microfluidics advantages are more efficiently exploited is in cell culturing.³⁰ *In vitro* cell cultures are currently the mainstay of experimental cell biological research for being the simplest model that sufficiently represents human biology and disease.³¹ Microfluidics provides systems for cell culturing that expand the capacity to, spatially and temporally, control local micro-environments, while minimizing potentially error-prone laboratory manipulations.³²

This motivation is the base of the biophotonic lab-on-a-chip (bioPhLoC) architecture that is described below.³³ This bioPhLoC allows a strict control of environmental conditions during cell proliferation and the simultaneous (and independent) analysis of cells and supernatant during the assay. To this end, the bioPhLoC is designed with two independent and fluidically connected (Figure 4a) chambers: the incubation and the monitoring chambers. The incubation chamber monolithically integrates $3 \mu\text{m}$ high microchannels (Figure 4b) which act as a size-exclusion microfilter. That is, small particles ($<3 \mu\text{m}$), such as *Escherichia coli* bacteria, can cross the filter, whereas big particles (e.g., yeasts or mammalian cells) will be retained in the incubation chamber. In the case of mammalian cell cultures this configuration is advantageous for several reasons. First, all cells

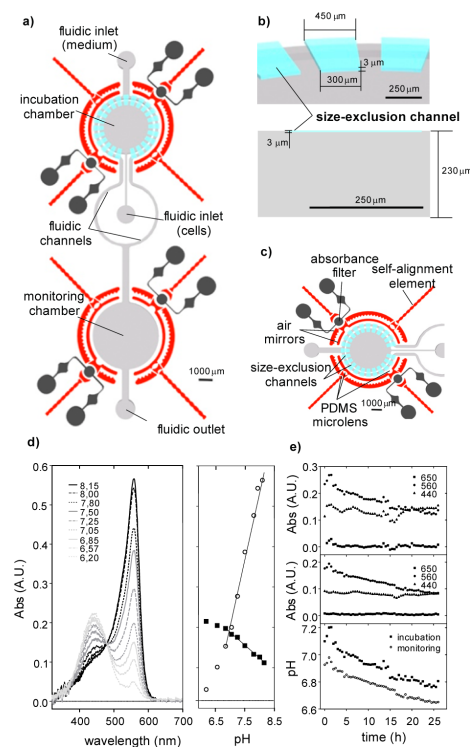


Figure 4. (a) Drawing of the bioPhLoC indicating the fluidic elements integrated on its structure (in gray in the figure); (b) 3D representation and cross section of the size-exclusion microchannels of the filter (in blue in the figure) integrated in the incubation chamber; (c) detail of the optical elements integrated in each chamber of the bioPhLoC; (d) absorbance spectra at wavelengths ranging from 350 to 900 nm for DMEM solutions at pH ranging from 8.15 to 6.20. The variation of the absorbance at wavelengths of 560 and 440 nm with the pH is also represented (Error bars show the standard deviation of three repetitive measurements.); (e) absorbance variation with time during seeding, trapping, and rinsing stages at wavelengths of 440, 560, and 650 nm, in the incubation (top) and monitoring chambers (medium). In the bottom plot, pH variation (from 560 nm wavelength) with time during seeding, trapping, and rinsing stages in the incubation and monitoring chambers. Figures published in ref 33 and reproduced by permission of The Royal Society of Chemistry. Copyright 2013.

inoculated will be retained and concentrated in the incubation chamber, which minimizes the number of cells lost during the experiment. Additionally, the presence of the filter restricts cell proliferation to the incubation chamber, improving the control of the culture and allowing the separated monitoring of cells and supernatant, without any additional separation process.

For cells and supernatant analysis, both chambers contain micro-optical elements for optical transduction analogous to the ones previously described, namely, self-alignment elements, collimation lenses, air mirrors for light confinement, and also include absorbance filters whose function will be described below (Figure 4c). The bioPhLoC is very versatile and allows colorimetric, dispersion, and/or fluorescence analysis of the

cells in the incubation chamber or the supernatant in the monitoring chamber. This can be achieved by just modifying the number and/or position of the fiber optics inserted in the system. That is, with a 180° configuration (fiber optics facing one another), it is possible to perform absorbance or scattering measurements, whereas at 90° it is possible to carry out fluorescence and/or wide angle dispersion analysis. Absorbance filters can be integrated in the bioPhLoC architecture by using sol-gel technology³⁴ and may improve fluorescence measurements by partially removing the excitation light from the collected signal, therefore increasing the SNR. The measurement of model molecules/particles (i.e., methylorenge, absorption at 470 nm, and *Escherichia coli*, dispersion at 600 nm) validates the performance of the micro-optical elements integrated therein for colorimetric and/or dispersion analysis.

Finally, the bioPhLoC is applied to the simultaneous detection of pH changes in the cells and the supernatant using vascular smooth muscle cells (VSMC) as model mammalian cells.

To this end, VSMC are trapped in the incubation chamber, where they proliferate under optimal experimental conditions (37 °C, 5% CO₂ and a low continuous flow of Dulbecco's Modified Eagle Medium (DMEM) at 0.5 μL min⁻¹ to avoid shear stress). During proliferation, cell metabolism transforms big substrates in small molecules such as CO₂ that acidify the culture medium. pH can be monitored by following the change of color of pH indicator phenol red already present in the culture medium. Concretely, phenol red presents two forms absorbing at 440 nm (protonated form) and 560 nm (deprotonated form), whose magnitude varies with the pH, as shown in Figure 4d. Thus, monitoring these absorption bands it is possible to follow pH changes in the culture medium with precision. The pH is determined through the 560 nm band for presenting higher sensitivities and low interference of other absorbing components of the medium (e.g., fetal bovine serum that absorbs at 390 nm).

In this case, pH is monitored in both incubation and monitoring chambers with a 180° configuration. Results are illustrated in Figure 4e. As shown, dispersion due to the attachment/detachment of cells interferes with the pH determination in the incubation chamber. Conversely, pH changes are determined in real-time, with precision and without interferences in the monitoring chamber.

Moreover, although control and monitoring of pH is a critical issue for cell engineering, this bioPhLoC may also be used to monitor other small or large molecules assimilated or secreted by cells. One interesting application may be the analysis of proteins, carbohydrates, or DNA/RNA secreted by cells. Detection of these molecules/compounds requires very energetic UV radiation.³⁵ As with bioPhLoC, cell proliferation and monitoring are performed in separated chambers, and secreted molecules can be measured in the monitoring chamber with high energetic UV light sources without compromising cell viability or the biological processes taking place there. Thus, bioPhLoC may be an ideal tool for secretomics, which is the analysis of secreted proteins of a culture.

Modular Optofluidic Configuration. The previous examples demonstrate that complex analytical systems can be developed for specific applications by monolithic integration of micro-optics with the microfluidic elements. While monolithic integration has undisputable benefits, reconfiguration requires an entirely new cycle of fabrication, from design to master fabrication and soft-lithography. Alternatively, a modular

Analytical Chemistry

Feature

approach can be pursued by separately fabricating functional units and achieve more flexibility for the user, postponing the assembly to the laboratory. The major challenge in this approach is to ensure the alignment of the optical axes during the assembly.

The Modular Optofluidic System (MOPS) represented in Figure 5 consists of several interchangeable pieces with distinct

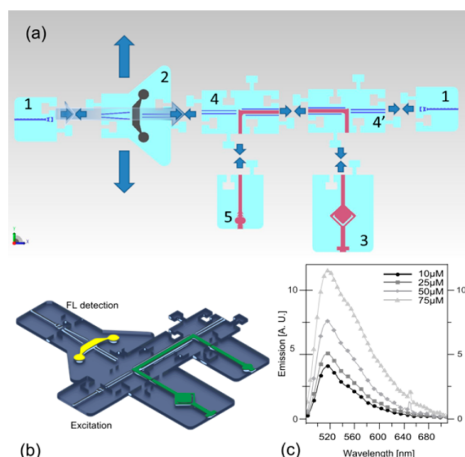


Figure 5. (a) Design-scheme of the MOPS used in this work. The individual modules are (1) two fiber optics connections, (2) a solid/liquid absorbance filter (filled with a colorant or a doped sol-gel) which can be included or excluded as required, (3) a fluidic inlet port with an internal air bubble based pressure regulator, (4/4') two waveguides directed to a microchannel which is shielded with air mirrors to prevent optical cross-talk, (5) a fluidic outlet port. (b) 90° Configuration for fluorescence measurements; (c) emission spectra of aqueous fluorescein solutions with different concentrations. Figures published in ref 36 and reproduced by permission of The Royal Society of Chemistry. Copyright 2014.

functions (Figure 5a) that can be easily assembled. All modules are fabricated using two-layer soft lithographic technology and each one exhibits plugs and sockets for reciprocal anchorage, thus ensuring optimal alignment and tight interconnections. Fluidic modules are plasma-bonded before use. The latter step, in combination with an air bubble based internal pressure regulator at the fluidic inlet (Figure 5a-3), allows obtaining a configurable-on-demand and completely leak-free microfluidic structure. The micro-optic modules are subsequently reversibly attached to the microfluidic structure and can be reconfigured according to the application. The system has been validated in proof-of-concept experiments for absorbance measurements in a 180° configuration using crystal violet as target analyte (as depicted in Figure 5a) and, as shown in Figure 5b,c, in a reconfigured 90° fluorescence configuration using fluorescein as target analyte. Here, excitation and detection axes are perpendicular to avoid background noise from nonabsorbed excitation radiation. An additional sol-gel absorbance filter³⁴ (module 2 in Figure 5a) blocks stray excitation radiation, further improving the SNR.

CONCLUSIONS

In this work we present fundamentals behind the design and operation of PhLoC based on the low-cost integration of three of the most widespread standard spectrophotometric analytical techniques: colorimetry in the UV-vis range, fluorimetry, and dispersion/scattering measurements. The fabrication of monolithically integrated micro-optic elements and its design only considering well-defined interphase surfaces and the refractive index variation among construction materials, surrounding air and analyte solutions has been explained and depicted through different PhLoC approaches dealing with common analytical problems. The use of micro-optic elements for light beam collimation has been presented, demonstrating to be extremely valuable for the boosting of light-sample interaction in optofluidic systems and therefore for the increase of the analytical sensitivity.

ASSOCIATED CONTENT

Supporting Information

The Supporting Information is available free of charge on the ACS Publications website at DOI: 10.1021/acs.anal-chem.6b00377.

Ready-to-use CAD design of microlenses and self-alignment channel for PDMS and pig-tailed fiber optics with NA = 0.22 (PDF)

AUTHOR INFORMATION

Corresponding Author

*E-mail: Andreu.llobera@imb-cnm.csic.es.

Author Contributions

I.R.-R. and T.N.A. equally contributed to this work. Both should be considered as first authors. The manuscript was written through contributions of all authors. All authors have given approval to the final version of the manuscript.

Notes

The authors declare no competing financial interest.

Biographies

Isaac Rodríguez-Ruiz has a Ph.D. in Chemistry (2013). He is currently a research fellow at the Laboratoire de Génie Chimique et Instrumentation (LGCI) at the French Alternative Energies and Atomic Energy Commission (DTEC/CEA-Marcoule). The main objects of his research are the development of novel analytical tools and photonic lab-on-a-chip platforms for precipitation studies related to hydrometallurgical processes and nuclear waste treatment.

Tobias N. Ackermann is currently a Ph.D. student at the Institut de Microelectrónica de Barcelona (CSIC). His studies are centered in the implementation of biological samples as photonic structures in photonic lab-on-a-chip platforms.

Xavier Muñoz-Berbel earned a Ph.D. in biotechnology (2008) and is a tenure-track researcher at the Institut de Microelectrónica de Barcelona (CSIC). His current research combines methodological, technological, and instrumental advances for biological science applications.

Andreu Llobera received a Ph.D. in Physics in 2002. Since 2009, he has held a permanent position as a researcher at the CSIC. He has coauthored more than 100 published articles. His research activities include integrated optics devices and photonic lab-on-a-chip platforms, either using silicon or polymer technology. Dr. Llobera was awarded a Starting Grant of the European Research Council in 2008.

6636

DOI: 10.1021/acs.analchem.6b00377
Anal. Chem. 2016, 88, 6630–6637

Analytical Chemistry

Feature

■ ACKNOWLEDGMENTS

This work has been partly funded by the European Commission (Contract No. 317916) under the LiPhos project. I.R. thanks the CEA-Enhanced Eurotalents Program for his Incoming CEA postdoctoral fellowship. X.M.B. acknowledges the MINECO for the award of a Ramón y Cajal contract.

■ REFERENCES

- (1) Manz, A.; Graber, N.; Widmer, H. *Sens. Actuators, B* **1990**, *1* (1), 244–248.
- (2) (a) Wu, M.-H.; Huang, S.-B.; Lee, G.-B. *Lab Chip* **2010**, *10* (8), 939–956. (b) Rodríguez-Ruiz, I.; Llobera, A.; Vila-Planas, J.; Johnson, D. W.; Gómez-Morales, J.; García-Ruiz, J. M. *Anal. Chem.* **2013**, *85* (20), 9678–9685.
- (3) Marcus, J. S.; Anderson, W. F.; Quake, S. R. *Anal. Chem.* **2006**, *78* (3), 956–958.
- (4) Martínez, A. W.; Phillips, S. T.; Whitesides, G. M.; Carrilho, E. *Anal. Chem.* **2010**, *82* (1), 3–10.
- (5) Shevkoplyas, S. S.; Yoshida, T.; Munn, L. L.; Bitensky, M. W. *Anal. Chem.* **2005**, *77* (3), 933–937.
- (6) Kimmel, D. W.; LeBlanc, G.; Meschievitz, M. E.; Cliffl, D. E. *Anal. Chem.* **2012**, *84* (2), 685–707.
- (7) Hoshino, K.; Huang, Y.-Y.; Lane, N.; Huebschman, M.; Uhr, J. W.; Frenkel, E. P.; Zhang, X. *Lab Chip* **2011**, *11* (20), 3449–3457.
- (8) Balslev, S.; Jorgensen, A.; Bilenberg, B.; Mogensen, K. B.; Snakenborg, D.; Geschke, O.; Kutter, J. P.; Kristensen, A. *Lab Chip* **2006**, *6* (2), 213–217.
- (9) Lepage, D.; Jiménez, A.; Beauvais, J.; Dubowski, J. J. *Light: Sci. Appl.* **2013**, *2* (4), e62.
- (10) (a) Psaltis, D.; Quake, S. R.; Yang, C. *Nature* **2006**, *442* (7101), 381–386. (b) Monat, C.; Domachuk, P.; Eggleton, B. *Nat. Photonics* **2007**, *1* (2), 106–114.
- (11) Llobera, A.; Demming, S.; Wilke, R.; Büttgenbach, S. *Lab Chip* **2007**, *7* (11), 1560–1566.
- (12) Mayers, B. T.; Vezenov, D. V.; Vullev, V. I.; Whitesides, G. M. *Anal. Chem.* **2005**, *77* (5), 1310–1316.
- (13) Müller, P.; Kopp, D.; Llobera, A.; Zappe, H. *Lab Chip* **2014**, *14* (4), 737–743.
- (14) Swinehart, D. F. *J. Chem. Educ.* **1962**, *39* (7), 333.
- (15) Valeur, B. *Molecular Fluorescence: Principles and Applications*; Wiley-VCH Verlag GmbH: Weinheim, Germany, 2001; Vol. 8.
- (16) Kwan, A.; Dudley, J.; Lantz, E. *Phys. World* **2002**, *15* (4), 64.
- (17) Vila-Planas, J.; Fernández-Rosas, E.; Ibarlucea, B.; Demming, S.; Nogués, C.; Plaza, J. A.; Domínguez, C.; Büttgenbach, S.; Llobera, A. *Nat. Protoc.* **2011**, *6* (10), 1642–1655.
- (18) Llobera, A.; Wilke, R.; Büttgenbach, S. *Talanta* **2008**, *75* (2), 473–479.
- (19) Llobera, A.; Wilke, R.; Büttgenbach, S. *Lab Chip* **2004**, *4* (1), 24–27.
- (20) Llobera, A.; Wilke, R.; Büttgenbach, S. *Lab Chip* **2005**, *5* (5), 506–511.
- (21) Ibarlucea, B.; Díez-Gil, C.; Ratera, I.; Veciana, J.; Caballero, A.; Zapata, F.; Tarraga, A.; Molina, P.; Demming, S.; Büttgenbach, S. *Analyst* **2013**, *138* (3), 839–844.
- (22) Gutiérrez, M.; Llobera, A.; Vila-Planas, J.; Capdevila, F.; Demming, S.; Büttgenbach, S.; Mínguez, S.; Jiménez-Jorquera, C. *Analyst* **2010**, *135* (7), 1718–1725.
- (23) Ibarlucea, B.; Fernández-Sánchez, C.; Demming, S.; Büttgenbach, S.; Llobera, A. *Analyst* **2011**, *136* (17), 3496–3502.
- (24) Long, G. L.; Winefordner, J. D. *Anal. Chem.* **1983**, *55* (7), 712A–724A.
- (25) Ordeig, O.; Ortiz, P.; Muñoz-Berbel, X.; Demming, S.; Büttgenbach, S.; Fernández-Sánchez, C. s.; Llobera, A. *Anal. Chem.* **2012**, *84* (8), 3546–3553.
- (26) Gutiérrez-Capitán, M.; Santiago, J.-L.; Vila-Planas, J.; Llobera, A.; Boso, S.; Gago, P.; Martínez, M.-C.; Jiménez-Jorquera, C. *J. Agric. Food Chem.* **2013**, *61* (39), 9325–9332.
- (27) Ibarlucea, B.; Fernández-Rosas, E.; Vila-Planas, J.; Demming, S.; Nogués, C.; Plaza, J. A.; Büttgenbach, S.; Llobera, A. *Anal. Chem.* **2010**, *82* (10), 4246–4251.
- (28) Llobera, A.; Juvert, J.; González-Fernández, A.; Ibarlucea, B.; Carregal-Romero, E.; Büttgenbach, S.; Fernández-Sánchez, C. *Light: Sci. Appl.* **2015**, *4* (4), e271.
- (29) Rodríguez-Ruiz, I.; Conejero-Muriel, M.; Ackermann, T. N.; Gavira, J. A.; Llobera, A. *Lab Chip* **2015**, *15* (4), 1133–1139.
- (30) El-Ali, J.; Sorger, P. K.; Jensen, K. F. *Nature* **2006**, *442* (7101), 403–411.
- (31) Meyvantsson, I.; Beebe, D. J. *Annu. Rev. Anal. Chem.* **2008**, *1*, 423–449.
- (32) Voldman, J.; Gray, M. L.; Schmidt, M. A. *Annu. Rev. Biomed. Eng.* **1999**, *1* (1), 401–425.
- (33) Muñoz-Berbel, X.; Rodríguez-Rodríguez, R.; Vigués, N.; Demming, S.; Mas, J.; Büttgenbach, S.; Verpoorte, E.; Ortiz, P.; Llobera, A. *Lab Chip* **2013**, *13* (21), 4239–4247.
- (34) Carregal-Romero, E.; Fernández-Sánchez, C.; Eguizabal, A.; Demming, S.; Büttgenbach, S.; Llobera, A. *Opt. Express* **2012**, *20* (21), 23700–23719.
- (35) (a) Vorndran, A.; Oefner, P.; Scherz, H.; Bonn, G. *Chromatographia* **1992**, *33* (3–4), 163–168. (b) Barbas, C. F.; Burton, D. R.; Scott, J. K.; Silverman, G. J. *Cold Spring Harbor Protocols* **2007**, 2007 (11), pdb.ip47.
- (36) Ackermann, T. N.; Álvarez-Conde, E.; Vila-Planas, J.; Müller, P.; Lorenz, T.; Dietzel, A.; Zappe, H.; Muñoz-Berbel, X.; Llobera, A. Modular optofluidic systems. In *microTAS 2014*, San Antonio, TX, 2014.

A.2 Publications based on derivative work

The following list of publications is a result of contributions, mostly in form of ray-tracing simulations but also some experimental work, which were based on the know-how acquired in the course of this thesis and motivated by curiosity and the opportunity provided by several collaborations to broaden my mind and field of expertise.

A.2.1 Journal articles

- S de Pedro, V J Cadarso, T N Ackermann, X Muñoz-Berbel, J A Plaza, J Brugger, S Büttgenbach, and A Llobera. Polymeric variable optical attenuators based on magnetic sensitive stimuli materials. *Journal of Micromechanics and Microengineering*, 24(12):125008, dec 2014. ISSN 0960-1317. doi: 10.1088/0960-1317/24/12/125008. URL <http://www.scopus.com/inward/record.url?eid=2-s2.0-84914693659{%&}partnerID=tZ0tx3y1>
- David Sanahuja, Pablo Gimenez-Gomez, Nuria Vignes, Tobias Nils Ackermann, Alfons Eduard Guerrero-Navarro, Ferran Pujol-Vila, Jordi Sacristan, Nidia Santamaria, Maria Sanchez-Contreras, Maria Diaz-Gonzalez, Jordi Mas, and Xavier Munoz-Berbel. Microbial trench-based optofluidic system for reagentless determination of phenolic compounds. *Lab on a chip*, 15(7):1717–1726, 2015. ISSN 1473-0189 (Electronic). doi: 10.1039/c4lc01446d. URL <http://dx.doi.org/10.1039/C4LC01446D>
- Isaac Rodríguez-Ruiz, Eduard Masvidal-Codina, Tobias Nils Ackermann, and Andreu Llobera. Photonic lab-on-chip (PhLOC) for enzyme-catalyzed reactions in continuous flow. *Microfluidics and Nanofluidics*, 18(5-6):1277–1286, 2015b. ISSN 1613-4982. URL <http://dx.doi.org/10.1007/s10404-014-1526-4>
- Ryo Usuba, Masatoshi Yokokawa, Tobias Nils Ackermann, Andreu Llobera, Kiyoshi Fukunaga, Soichiro Murata, Nobuhiro Ohkohchi, and Hiroaki Suzuki. Photonic Lab-on-a-Chip for Rapid Cytokine Detection. *ACS Sensors*, 1(8):979–986, 2016. ISSN 23793694. doi: 10.1021/acssensors.6b00193. URL <http://dx.doi.org/10.1021/acssensors.6b00193>

A.2.2 Conferences

- Sandra De Pedro, Tobias N. Ackermann, Jose A. Plaza, Erica Alvarez, Stephanus Büttgenbach, Victor J. Cadarso, and Andreu Llobera. All-photonic SU-8 Variable Optical Attenuator. In *International Conference on Optical MEMS and Nanophotonics*, pages 63–

64. IEEE, aug 2014. ISBN 9780992841423. doi: 10.1109/OMN.2014.6924544. URL <http://dx.doi.org/10.1109/OMN.2014.6924544>
- Tobias N Ackermann, Jordi Vila-planas, Xavier Muñoz-berbel, Erica Álvarez-conde, Daniel Kopp, Hans Zappe, and Andreu Llobera. Modular optofluidic systems : A toolbox for fast and simple assembly of a photonic lab on a chip . pages 21–22, San Jose, California (USA), 2016b. CLEO:2016. ISBN 9781943580118
 - Tobias N. Ackermann, Jiri Dietvorst, Ana Sanchis, Juan P. Salvador, Xavier Munoz-Berbel, Erica Alvarez-Conde, Daniel Kopp, Hans Zappe, M.-Pilar Marco, and Andreu Llobera. Modular Optofluidic Systems (MOPS). In *μTAS 2014, San Antonio Texas*, page 100131C, 2016c. ISBN 9780979806476. doi: 10.1117/12.2242997. URL <http://proceedings.spiedigitallibrary.org/proceeding.aspx?doi=10.1117/12.2242997>
 - Isaac Rodríguez-Ruiz, Mayte Conejero-Muriel, Tobias N. Ackermann, José A. Gavira, and Andreu Llobera. A multiple path photonic lab on a chip for parallel protein concentration measurements. In *Lab Chip*, volume 15, pages 1133–1139, 2015a. ISBN 9780979806476. doi: 10.1039/C4LC01332H. URL <http://xlink.rsc.org/?DOI=C4LC01332H>

B.0.1 Python for data acquisition and processing

My Optics Lab

```
# -*- coding: utf-8 -*-
```

```
'''
```

```
Created on Sun Sep 18 19:18:16 2016
```

```
@author: nils
```

```
Script initializing the laboratory equipment providing functions for measurement  
and control.
```

```
'''
```

```
class MyOpticsLab:
```

```
'''
```

```
Provides control of a number of Ocean Optics devices and the PI
```

```
Eco Corvus motor stage.
```

```
Calling the function MyLab_init(Spectrometers=True, Stage=False)
```

takes care of initializing all connected devices, Stage initialization is deactivated by default though. To use it set Stage=True.

Requires

```
seabreeze with backend 'cseabreeze'  
(https://github.com/ap--/python-seabreeze)
```

for instantiation.

» » »

```
SeaBreeze_dict={ '<SeaBreezeDevice USB4000:FLMT00119>': 'flame',  
                  '<SeaBreezeDevice USB2000PLUS:USB2+F04041>': 'USB2000plus',  
                  '<SeaBreezeDevice USB2000PLUS:USB2+H02391>': 'USB2000plusXR',  
                  '<SeaBreezeDevice QE65000:QEPB0195>': 'QE65Pro',  
                  '<SeaBreezeDevice QE-PRO:QEP00913>': 'QEPro',  
                  '<SeaBreezeDevice QE65000:QEB0653>': 'QE65000',  
                  '<SeaBreezeDevice HR4000:HR4C2550>': 'HR4000',  
                  '<SeaBreezeDevice MAYA2000:MAY11044>': 'Maya' }
```

```
OO_symlinks = { 'flame': 'usb4000-',  
                'QE65Pro': 'qe65000+-',  
                'QE65000': 'qe65000+-',  
                'QEPro': 'qepro+-',  
                'USB2000': 'usb2000-',  
                'USB2000plus': 'usb2000+-',  
                'USB2000plusXR': 'usb2000+-',  
                'Nirquest256': 'nirquest256-',  
                'Nirquest512': 'nirquest512-',  
                'HR4000': 'hr4000-',  
                'Maya': 'maya2000-',  
                'MayaPro': 'mayapro2000-' }
```

```
List=[]
```

```
import matplotlib.gridspec as gridspec
```

```
gs = gridspec.GridSpec(7, 7)
```

```
IT = 15
```

```

IT1 = 15
IT2 = 15
using_TTLshutter = False

def __init__(self, os, sl, sbs):
    import getpass
    user = getpass.getuser()

    import pprint
    pp=pprint.PrettyPrinter(indent=4)
    print('\n hello ' + user + ' ! welcome to LabOptica :)')

    try:
        self.devices = sbs.list_devices()

    except sbs.SeaBreezeError:
        print('\n Permission error... grant permission:\n')
        self.search_Spectrometers(os, user)
        self.devices = sbs.list_devices()
        print('\n The following Ocean Optics devices have been recognized:'
              '\n')
        pp.pprint(self.devices)
    else:
        print('\n The following Ocean Optics devices have been recognized:'
              '\n ')

        pp.pprint(self.devices)
#         print('search for Ocean Optics devices using their label,'
#               'e. g. "flame" or "QE65Pro"')

def get_permission(self, os, symlink, user):
    import time
    command = 'gnome-terminal -e \'sudo chown %s:%s /dev/%s\'' % (
        user, user, symlink)

```

```

command_R = 'gnome-terminal -e \'sudo chown -R %s:%s /dev/%s\'' % (
    user, user, symlink)

print(command)
print(command_R)
os.system(command)
time.sleep(2)
os.system(command_R)
time.sleep(2)

def search_Spectrometers(self, os, user):
    """
    works for max. 2 spectrometers of the same type connected at the same
    time
    """
    user = user
    ## call list command ##
    import subprocess
    p = subprocess.Popen("cd /dev && ls", stdout=subprocess.PIPE,
                          shell=True)
    (output, err) = p.communicate()
    ## Wait for date to terminate. Get return returncode ##
    p_status = p.wait()
    print("Command output : ")
    #pp.pprint(output.split(b'\n'))
    print("\n Command exit status/return code : ", p_status)
    out = str(output, encoding='UTF-8')

    for name in self.OO_symlinks.values():
        start_index = out.find(name)
        if start_index > -1:
            di=len(name)
            end_index = start_index + di + 2
            symlink = out[start_index:end_index].split('\n')[0]
            self.List.append(symlink)
            self.get_permission(os, symlink, user)

```

```

        #check if there is another Spectrometer of the same type:
        out_tail = out.split(symlink)[1]
        start_index = out_tail.find(name)
        if start_index > -1:
            di=len(name)
            end_index = start_index + di+2
            symlink = out_tail[start_index:end_index].split('\n')[0]
            self.List.append(symlink)
            self.get_permission(os, symlink, user)
        print(self.List)

def init_spec(self, label, index):
    self.label = MySpectrometer(index)

###-----#

def single_spec_ani(self, i):
    #import matplotlib.pyplot as plt

    from matplotlib import style
    #style.use('seaborn-dark-palette')
    style.use('bmh')
    sp.set_IT(MyLab.IT)

    #self.ax = fig.add_subplot(2,2,locate)
    WL_array = sp.WL
    Intensities = sp.get_signal()

    self.ax.clear()
    self.ax.set_title(self.SeaBreeze_dict[str(MyLab.devices[0])],
                                fontsize=9)

    self.ax.plot(WL_array, Intensities)

###-----#

def double_spec_ani_left(self, i):

```



```
#import matplotlib.pyplot as plt

from matplotlib import style
#style.use('seaborn-dark-palette')
style.use('bmh')

sp1.set_IT(MyLab.IT1)
#self.ax = fig.add_subplot(2,2,locate)
WL_array = sp1.WL[100:-100]
Intensities = sp1.get_signal()[100:-100]

self.ax1.clear()
self.ax1.set_title(self.SeaBreeze_dict[str(MyLab.devices[0])],
                    fontsize=9)

self.ax1.plot(WL_array, Intensities)

def double_spec_ani_right(self, i):
    #import matplotlib.pyplot as plt

    from matplotlib import style
    #style.use('seaborn-dark-palette')
    style.use('bmh')
    sp2.set_IT(MyLab.IT2)

    #self.ax = fig.add_subplot(2,2,locate)
    WL_array = sp2.WL[100:-100]
    Intensities = sp2.get_signal()[100:-100]

    self.ax2.clear()
    self.ax2.set_title(self.SeaBreeze_dict[str(MyLab.devices[1])],
                        fontsize=9)

    self.ax2.plot(WL_array, Intensities)

###-----#
```

```

def SingleSpecAnimation(self):

    self.fig_single = plt.figure()
    self.ax = self.fig_single.add_subplot(self.gs[0:6,0:6])
    import matplotlib.animation as animation
    ani = animation.FuncAnimation(self.fig_single, self.single_spec_ani,
                                  interval = 1000)

    plt.show()

    return ani

def DoubleSpecAnimation(self):

    self.fig_double = plt.figure()
    self.ax1 = self.fig_double.add_subplot(self.gs[0:7,0:3])
    self.ax1.yaxis.tick_left()
    self.ax2 = self.fig_double.add_subplot(self.gs[0:7,4:7])
    self.ax2.yaxis.tick_right()
    import matplotlib.animation as animation
    ani1 = animation.FuncAnimation(
        self.fig_double, self.double_spec_ani_left, interval = 1000)
    ani2 = animation.FuncAnimation(
        self.fig_double, self.double_spec_ani_right, interval = 1000)
    plt.show()

    return ani1, ani2

###-----#

def spectrometers_init(self):
    from MySpectrometer import MySpectrometer
    self.NonlinCorrect = False
    self.DarkCurrentCorrect = False

    if len(self.devices)==1:

```

```
try:
    open_Specs = [sp]
except NameError:
    open_Specs = np.zeros(len(self.devices))

sp = MySpectrometer(sb, sbs, self, self.devices[0], open_Specs[0])
sp.set_IT(self.IT)
if (self.SeaBreeze_dict[str(self.devices[0])] == 'USB2000plus'
or self.SeaBreeze_dict[str(self.devices[0])] == 'QE65Pro'
or self.SeaBreeze_dict[str(self.devices[0])] == 'Maya'):
    self.light_switch = sp
print('Ocean Optics Spectrometer '
      + self.SeaBreeze_dict[str(self.devices[0])]
      + ' can be called upon as "sp"')

outer_ani = self.SingleSpecAnimation()
plt.show()

elif len(self.devices)==2:

    try:
        open_Specs = [sp1, sp2]
    except NameError:
        open_Specs = np.zeros(len(self.devices))

    sp1 = MySpectrometer(sb, sbs, self, self.devices[0], open_Specs[0])
    sp1.set_IT(self.IT1)
    if self.SeaBreeze_dict[str(self.devices[0])] in ['USB2000plus',
                                                    'QE65Pro', 'Maya']:

        self.light_switch = sp1
    print('\n Ocean Optics Spectrometer '
          + self.SeaBreeze_dict[str(self.devices[0])]
          + ' can be called upon as "sp1"')
```

```

        sp2 = MySpectrometer(sb, sbs, self, self.devices[1], open_Specs[1])
        sp2.set_IT(self.IT2)
        if self.SeaBreeze_dict[str(self.devices[1])] in ['USB2000plus',
                                                         'QE65Pro', 'Maya']:

            self.light_switch = sp2

        print('\n Ocean Optics Spectrometer "' +
              self.SeaBreeze_dict[str(self.devices[1])]
              + '" can be called upon as "sp2"')
        open_Specs = [sp1, sp2]
        outer_ani = self.DoubleSpecAnimation()

        plt.show()

###-----#

def axes_init(self, axes = ['1', '2', '3']):

    self.axis = {}
    for key in axes:
        self.axes[key]= MyAxis(key, self.Stage)

    if self.Stage.isOpen():
        print('\n Connection to Stage successfully established')

### -----#

def Cam(self, os, number_as_string):

    command = 'gnome-terminal -e \'sudo xawtv -gl -xv -vm -device \'
               '/dev/video%s' % (number_as_string)

    os.system(command)

### -----#

def MyLab_init(Spectrometers = True, Stage=False, axes=['1','2','3'],
               n_xips = 1):

```

```
import os as os
import matplotlib as mpl
import matplotlib.pyplot as plt
import numpy as np

import serial as sl
import seabreeze as sb
sb.use('cseabreeze')
import seabreeze.spectrometers as sbs

global MyLab
### invoke and initialize MyLabOptica instance
MyLab = MyOpticsLab(os, sl, sbs)

### in case of various measurement positions:
MyLab.n_xips = n_xips

'''
init Stage
'''

if Stage:

    from MyStage_ import MyStage, MyAxis

    MyLab.Stage = MyStage(os, sl, MyLab.n_xips)
    MyLab.Stage.connect()
    MyLab.axes_init()

'''
init Spectrometers, call animation of spectrometer intensities
'''

if Spectrometers:
```

```
MyLab.spectrometers_init()
```

```
####-----####
'''
if __name__ == "__main__":

    from MyOpticsLab import MyOpticsLab
    MyOpticsLab.MyLab_init()
'''
```

Spectrometer Control

```
# -*- coding: utf-8 -*-
'''

Created on Wed Jun 22 23:53:59 2016

@author: nils
'''

import numpy as np

class MySpectrometer(object):

    #import seabreeze
    #seabreeze.use('cseabreeze')

    def __init__(self, sb, sbs, parent, device, open_device):

        try:

            self.access = sbs.Spectrometer(device)

        except sbs.SeaBreezeError:

            self.access = open_device.access

        self.WL = self.access.wavelengths()
```

```
#create dictionary with WL and corersponding indexes to access index
#of given wavelength key
WL_keys = tuple(self.WL)
WL_indeces = tuple(list(range(0,len(self.WL))))
self.WL_dict = {WL_keys[i]:WL_indeces for i in list(
    range(0,len(self.WL)))}
self.parent = parent

def close(self):

    self.access.close()

def light_on(self):

    if self.parent.using_TTLshutter:
        self.access.lamp_set_enable(False)
    else:
        self.access.lamp_set_enable(True)

def light_off(self):

    if self.parent.using_TTLshutter:
        self.access.lamp_set_enable(True)
    else:
        self.access.lamp_set_enable(False)

def set_IT(self, integration_time_milisc):

    integration_time = 1000*integration_time_milisc
    #self.parent.IT = integration_time
    self.access.integration_time_micros(integration_time)

def get_signal(self):

    return self.access.intensities(
```

```

        correct_dark_counts=self.parent.DarkCurrentCorrect,
        correct_nonlinearity=self.parent.NonlinCorrect)

def get_dark(self):

    self.access.lamp_set_enable(False)

    return self.access.intensities(
        correct_dark_counts=self.parent.DarkCurrentCorrect,
        correct_nonlinearity=self.parent.NonlinCorrect)

def acquire_clean_signal(self):
    import time

    # apply settings
    #acquire the data
    self.parent.light_switch.light_off()
    time.sleep(.075)
    dark1 = []
    for i in range(4):
        dark1.append(self.get_signal())
    dark1 = np.average(dark1[1:], axis=0)

    self.parent.light_switch.light_on()
    time.sleep(.075)
    noisy_signal= []
    for i in range(4):
        noisy_signal.append(self.get_signal())
    noisy_signal= np.average(noisy_signal[1:], axis=0)

    #self.spectrum(correct_dark_counts=True, correct_nonlinearity=True)
    #returns
    #numpy.vstack of wavelengths and intensities

```



```

        self.parent.light_switch.light_off()

        time.sleep(.075)
        dark2 = []
        for i in range(4):
            dark2.append(self.get_signal())
        dark2 = np.average(dark2[1:], axis=0)
        #do the arithmetics
        dark = (dark1 + dark2)/2
        clean_signal = noisy_signal - dark

        return np.array(clean_signal)

def avg_spec(self, n):

    spectra=[]
    for i in range(n):
        spectra.append(self.get_signal())
    yerr = np.nanstd(spectra, axis=0)
    mean = np.nanmean(spectra, axis=0)

    return {'mean spec':mean, 'std dev':yerr, 'N':n, 'IT':self.parent.IT}

def avg_dark_corrected(self, n):
    """
    interactive semi-automatic spectrum acquisition with dark correction
    """
    import time
    input('please turn the lightsource OFF ')
    time.sleep(self.parent.IT/1000)
    dark = self.avg_spec(n)

    input('Saved dark. Now, please turn the lightsource ON ')
    time.sleep(self.parent.IT/1000)
    i = self.avg_spec(n)

```

```

i['dark'] = dark['mean spec']

i_corrected = i['mean spec'] - dark['mean spec']
i['mean spec'] = i_corrected

return i

print('Dark-corrected intensity acquired.')

###-----###

```

Motor Stage Control

```

# -*- coding: utf-8 -*-
"""
Created on Thu Aug 11 13:00:08 2016

@author: nils

### 'python3 -m serial.tools.list_ports' executed in terminal lists the
available ports
### ttyS0,ttyS1 are the linux equivalent to COM1, COM2, so for example use
#serialport = '/dev/ttyUSB0'
#corvus.baudrate = 57600
#corvus.open()
#print('Corvus port is open? '+str(corvus.isOpen()))

This file is adapted from Micos.py ()
by Philipp Klaus and adjusted to control the
Micos Corvus Eco
The original file header is cited following:

# Author: Philipp Klaus, philipp.l.klaus AT web.de

```

B. SOFTWARE CODE

```
# This file is part of Micos.py.

#

# Micos.py is free software: you can redistribute it and/or modify
# it under the terms of the GNU General Public License as published by
# the Free Software Foundation, either version 3 of the License, or
# (at your option) any later version.

#

# Micos.py is distributed in the hope that it will be useful,
# but WITHOUT ANY WARRANTY; without even the implied warranty of
# MERCHANTABILITY or FITNESS FOR A PARTICULAR PURPOSE. See the
# GNU General Public License for more details.

#

# You should have received a copy of the GNU General Public License
# along with Micos.py. If not, see <http://www.gnu.org/licenses/>.

### This module depends on PySerial, a cross platform Python module
### to leverage the communication with the serial port.
### http://pyserial.sourceforge.net/pyserial.html#installation
### If you have 'pip' installed on your computer, getting PySerial is as easy
### as
### pip install pyserial

'''

class MyStage(object):

    TIMEOUT = 0.05

    DEBUG = False

    serialPort = ''

    def __init__(self, os, serial_module, n_xips):

        self.os = os

        self.sl = serial_module

        self.n_xips = n_xips

        self.positions_set = [False for pos in range(self.n_xips)]
```

```

connection = None

print('\n Stage module loaded - do "dmesg | grep tty" to list Ports of'
      'connected serial devices:\n')

import subprocess
import pprint
pp=pprint.PrettyPrinter(indent=4)

## call date command ##
p = subprocess.Popen("dmesg | grep tty", stdout=subprocess.PIPE,
                     shell=True)

(output, err) = p.communicate()

# Wait for date to terminate. Get return returncode, which should
# look something like:
"""
Command output :
[  b'[    0.000000] console [tty0] enabled',
  b'[    0.475694] 00:07: ttyS0 at I/O 0x3f8 (irq = 4,
    base_baud = 115200) i'
  b's a 16550A',
  b'[    0.498016] 0000:00:03.3: ttyS4 at I/O 0x1c88 (irq = 17,
    base_baud = '
  b'115200) is a 16550A',
  b'[    8.763219] usb 7-2: FTDI USB Serial Device converter now
    attached to'
  b' ttyUSB0',
  b'' ] ##
"""

p_status = p.wait()
print("Port from output : ")
port = '/dev/' + str(output.split(b'\n')[-2])[-8:-1]
try:
    self.serialPort = port
    print('\n Try to connect to SerialPort: \n' + self.serialPort)

```

```
        self.connect(self.serialPort)

    except self.sl.serialutil.SerialException as se:
        raise CorvusError(se)

def connect(self, serialPort, baud=57600):

    try:
        self.connection = self.sl.Serial(serialPort, baudrate=baud,
                                           bytesize=8, parity='N',
                                           stopbits=1, xonxoff=False,
                                           rtscts=False, write_timeout=None,
                                           dsrdtr=False,
                                           timeout=self.TIMEOUT)
    except self.sl.serialutil.SerialException as se:
        #raise CorvusError(se)
        self.get_permission(serialPort)#
        import time
        time.sleep(3)
        self.connection = self.sl.Serial(serialPort, baudrate=baud,
                                           bytesize=8, parity='N',
                                           stopbits=1, xonxoff=False,
                                           rtscts=False, write_timeout=None,
                                           dsrdtr=False,
                                           timeout=self.TIMEOUT)

def get_permission(self, serialPort):

    command = 'gnome-terminal -e \'sudo chmod 666 %s\'' % (serialPort)
    #serialPort = '/dev/tty%s' % (USBport)
    self.os.system(command)

def isOpen(self):
    #self.debugMessage(what)
    return self.connection.isOpen()
```

```

def user_init(self):

    ### start sending venus1 commands to corvus
    self.write(b'0_mode_') # setting the stage in Host-mode, where commands
    # have to end with a '_' (space)
    self.write(b'restore_') # loads the last saved settings
    self.write(b'3_setdim_') # set dimensions
    self.write(b'1_1_setaxis_')
    self.write(b'1_2_setaxis_')
    self.write(b'1_3_setaxis_') # makes sure that the axes are turned on
    self.write(b'2_1_setunit_')
    self.write(b'2_2_setunit_')
    self.write(b'2_3_setunit_') # sets units to mm for all the axes

    #Stage.write(b'0_0_0_m_') # moves to the stored Origin
    #Stage.write(b'0_0_0_setpos_') # sets Origin at current position

def set_home(self):

    # the next line initializes the internal step tracking of MyAxis
    self.positions_set[0] = not self.positions_set[0]
    print('home_set is set to ' + str(self.positions_set[0]))
    # ...the ordinary set home command in Venus1 language:
    self.write(b'0_0_0_setpos_')

def set_positions(self):

    self.positions_set = [not pos for pos in self.positions_set]
    print('All positions set. Monitoring can be started. ')

def get_pos(self):

    self.write(b'pos_')
    self.read()

def save(self):

```

```
        self.write(b'save_')

        # saves settings on Corvus memory for next session

def send(self, command, numEnquiries = 1):
    self.connection.flushInput()
    self.write(command)
    #if mnemonic != C['ETX']: self.read()
    #self.read()
    #self.getACQorNAK() # try with this line commented
    response = []
    for i in range(numEnquiries):
        #self.enquire()
        response.append(self.read())
    return response

def write(self, what):
    #self.debugMessage(what)
    self.connection.write(what)

def read(self):
    response = self.connection.read()
    return response

def close(self):
    #self.debugMessage(what)
    self.connection.close()

class MyAxis(object):

    #sidestep = [0,0,0]

    def __init__(self, axis_number, parent):
        self.name = 'Axis' + axis_number
        self.axis_number = axis_number
```

```

        self.parent = parent
        self.step_down = [0 for n in range(self.parent.n_xips)]
        self.step_out = [0 for n in range(self.parent.n_xips)]
        self.step_in = [0 for n in range(self.parent.n_xips)]

def send(self, command):
    #command = command.replace('AX', self.axis_number)
    return self.parent.send(command)

#def actual_position(self):
    #return self.send(b'AX_np_')

#def homing(self):
    ### homing (search limit reverse)
    #return self.send('AX_ncal_')

def move_relative(self, by):
    if self.axis_number == '1':
        self.send(b'%f_0_0_r_' % (by))
    elif self.axis_number == '2':
        self.send(b'0_%f_0_r_' % (by))
    elif self.axis_number == '3':
        self.send(b'0_0_%f_r_' % (by))
    else:
        print('Error: Axis numer out of range.')

# Next we define specific movements with the aim of creating an internal
# (class owned) memory for the movements performed after the boolean
# variables "home_set" and "step1_set" respectively have been set to "True"
# The steps thus defined can be called upon afterwards from by the
# monitoring cycle to carry out the correct movements at each step.

def move_out(self, by):

    #if activated by MyStage.set_home(), the next lines create an internal

```



```
# step tracking
if (self.parent.positions_set[0] == True
    and not self.parent.positions_set[1] == True):
    if self.axis_number == '2':
        self.step_in[0] = self.step_in[0] - by
        self.send(b'0_-%f_0_r_' % (by))
    else:
        print('Error: Axis number not defined for that movement')

elif (self.parent.positions_set[0] == True
    and self.parent.positions_set[1] == True
    and not self.parent.positions_set[2] == True):
    if self.axis_number == '2':
        self.step_in[1] = self.step_in[1] - by
        self.send(b'0_-%f_0_r_' % (by))
    else:
        print('Error: Axis number not defined for that movement')

elif (self.parent.positions_set[0] == True
    and self.parent.positions_set[1] == True
    and self.parent.positions_set[2] == True):
    if self.axis_number == '2':
        self.step_in[2] = self.step_in[2] - by
        self.send(b'0_-%f_0_r_' % (by))
    else:
        print('Error: Axis number not defined for that movement')

# if step tracking is not needed, the ordinary command is executed:
else:
    if self.axis_number == '2':
        self.send(b'0_-%f_0_r_' % (by))
    else:
        print('Error: Axis number not defined for that movement')

def move_up(self, by):
```

```

if (self.parent.positions_set[0] == True
    and self.parent.positions_set[1:] == [False for value in
                                            self.parent.positions_set[1:]]):
    if self.axis_number == '3':
        self.step_down[0] = self.step_down[0] - by
        self.send(b'0_0_-%f_r_' % (by))
    else:
        print('Error: Axis number not defined for that movement.')

elif (self.parent.positions_set[:1] == [True for value in
                                          self.parent.positions_set[:1]]
      and self.parent.positions_set[2:] == [False for value in
                                              self.parent.positions_set[2:]]):
    if self.axis_number == '3':
        self.step_down[1] = self.step_down[1] - by
        self.send(b'0_0_-%f_r_' % (by))
    else:
        print('Error: Axis number not defined for that movement.')

elif (self.parent.positions_set[:2] == [True for value in
                                          self.parent.positions_set[:2]]
      and self.parent.positions_set[3:] == [False for value in
                                              self.parent.positions_set[3:]]):
    if self.axis_number == '3':
        self.step_down[2] = self.step_down[2] - by
        self.send(b'0_0_-%f_r_' % (by))
    else:
        print('Error: Axis number not defined for that movement.')

else:
    if self.axis_number == '3':
        self.send(b'0_0_-%f_r_' % (by))
    else:
        print('Error: Axis number not defined for that movement.')

```

```
def move_down(self, by):

    if (self.parent.positions_set[0] == True
        and self.parent.positions_set[1:] == [False for value in
                                                self.parent.positions_set[1:]]):
        if self.axis_number == '3':
            self.step_down[0] = self.step_down[0] + by
            self.send(b'0_0_%f_r_' % (by))
        else:
            print('Error: Axis number not defined for that movement.')

    elif (self.parent.positions_set[:1] == [True for value in
                                             self.parent.positions_set[:1]]
          and self.parent.positions_set[2:] == [False for value in
                                                  self.parent.positions_set[2:]]):
        if self.axis_number == '3':
            self.step_down[1] = self.step_down[1] + by
            self.send(b'0_0_%f_r_' % (by))
        else:
            print('Error: Axis number not defined for that movement.')

    elif (self.parent.positions_set[:2] == [True for value in
                                             self.parent.positions_set[:2]]
          and self.parent.positions_set[3:] == [False for value in
                                                  self.parent.positions_set[3:]]):
        if self.axis_number == '3':
            self.step_down[2] = self.step_down[2] + by
            self.send(b'0_0_%f_r_' % (by))
        else:
            print('Error: Axis number not defined for that movement.')

    else:
        if self.axis_number == '3':
            self.send(b'0_0_%f_r_' % (by))
        else:
```

```

        print('Error: Axis number not defined for that movement')

def move_in(self, by):

    if (self.parent.positions_set[0] == True
        and not self.parent.positions_set[1] == True):
        if self.axis_number == '2':
            self.step_in[0] = self.step_in[0] + by
            self.send(b'0_%f_0_r_' % (by))
        else:
            print('Error: Axis number not defined for that movement')

    elif (self.parent.positions_set[0] == True
          and self.parent.positions_set[1] == True
          and not self.parent.positions_set[2] == True):
        if self.axis_number == '2':
            self.step_in[1] = self.step_in[1] + by
            self.send(b'0_%f_0_r_' % (by))
        else:
            print('Error: Axis number not defined for that movement')

    elif (self.parent.positions_set[0] == True
          and self.parent.positions_set[1] == True
          and self.parent.positions_set[2] == True):
        if self.axis_number == '2':
            self.step_in[2] = self.step_in[2] + by
            self.send(b'0_%f_0_r_' % (by))
        else:
            print('Error: Axis number not defined for that movement')

    else:
        if self.axis_number == '2':
            self.send(b'0_%f_0_r_' % (by))
        else:
            print('Error: Axis number not defined for that movement')

```

```
"""
def move_absolute(self, to):
    if self.axis_number == '1':
        self.send(b'%f_0_0_m_' % (to))
    elif self.axis_number == '2':
        self.send(b'0_%f_0_m_' % (to))
    elif self.axis_number == '3':
        self.send(b'0_0_%f_m_' % (to))
    else:
        print('Error: Axis numer out of range.')
"""

### ----- now we define the exceptions that could occur -----

class MicosError(Exception):
    pass

class CorvusError(MicosError):
    pass
```

C.1 SU-8 Masters

General Fabrication sequence for SU-8 masters on silicon wafers:

1. Dehydration bake of double-sided polished wafers for 15minute (min) at 100°C
2. Clean masks with acetone and dry with nitrogen
3. 5µm thick layer of SU8-2005 (up to 25 µm thickness) for better adhesion of the following layers:
 - spincoat in two steps: 15second (sec) at 400 rpm for homogenisation, 30sec at 3000 rpm
 - softbake with ramp from 65°C to 90°C (37.5% power for heating to achieve ramp in 15)
 - float exposure at dose of 70 mJ/cm² (7sec with Mask-aligner (Karl Süss MA6) at 11 mW/cm² lamp-power)
 - post-exposure bake from 65°C to 85°C in 15'
4. O₂-plasma (500 W, 0.8 mbar, 18sec) for activation of surface before depositing next layer
5. Following layers with SU8-2050 to achieve thicker layers (up to 500 µm thickness):
 - spincoating at 700 rpm for 230 µm thickness, dose to clear 320 mJ/cm²

¹applied only if next layer is to be thick

- spincoating at 1200 rpm for 125 μm thickness, dose to clear 275 mJ/cm^2

C.2 MY-polymer processing

C.2.1 Curing of MY-polymers (MY-polymer (MY-polymer)s)

Manufacturer input: Inertion essential, dose between 1000-2000 mJ/cm^2 sufficient, above 2000 mJ/cm^2 ($\geq 4\text{min}$, as Mask-aligner KS MA6 gives 11mW/s) recommended.

C.2.1.1 In PDMS on glass (no primer, no additional inertion)

PDMS molds on glass were filled with MY-133 V2000 or MY-132 A and left over one hour. Exposure for 4min without effect, no polymerization. Subsequent additional 15 min without effect either.

\Rightarrow once exposed under oxygen-presence, the oxygen binds radicals and the polymerisation-reaction cannot take place.

C.2.1.2 On glass (no primer)

MY-133 V2000 or MY-132 A and exposed to UV-light within half an hour for 4min

- under water:
perfect polymerisation.
- in PDMS-mold in air:
no polymerisation.
- in PDMS-mold under water:
no polymerisation.

C.2.1.3 On glass in PDMS-mold (MY-polymer attached to glass)

Glass-slide was pre-coated with Primer G via air-brush, after 10min PDMS-molds were attached to the coated surface and filled with MY-133 V2000 and MY-132 A respectively. Samples were exposed to UV-light within 20min after filling the structures (KS MA6 for 10min).

Results: Successful soft-lithography, details in Master-thesis

C.2.1.4 Inside PDMS-chip

Fabrication inside the two parts of a PDMS-chip with the same parameters as in C.2.1.3 with and without coating with Primer G.

Curing only partly successful; some areas perfect, others liquid. Performance probably disturbed by some kind of contamination of the PDMS-molds previous to MY-injection.

C.2.1.5 In SU-8 Master (no primer, water-inertion)

MY-132 A injected in SU-8 master on silicon wafer was inerted (master with polymer was set under water) within 20min after first exposure to air and subsequently exposed to UV-light for 10min.

Curing successful, polymer-pieces could be peeled off the master entirely.

C.2.1.6 On glass in PDMS-mould (MY-polymer attached to PDMS)

see C.2.2.3

C.2.2 PDMS-chips with MY-channel-bottom ('Hybrids')

C.2.2.1 PDMS-parts of chips

PDMS-parts of chips with fluidic channels and optics of 62.5µm height were fabricated with standard soft-lithography using SU8-masters according to lower part of LiPhos-Mask mypReactor.

C.2.2.2 Coating with Primer G and injection molding of MY-polymers

PDMS-parts with micro-channels were airbrush-coated with Primer G and the surface subsequently cleaned with a towel and acetone such that Primer G was only left inside the micro-channels. MY-injection and -curing was done under water according to ???. After curing, PDMS-parts could be removed from glass without leaving MY-rests there \Rightarrow *process successful*

Observations:

- bonding of MY-polymers (both types) to PDMS not good, mainly supported by the sticky character of the surfaces. Cured MY-polymer could be removed easily with tweezers from inside the channels.
- as PDMS-molds are not bonded properly to glass-slides, MY-polymer tends to enter not only the micro-channels, but also optical elements and alignment structures, especially when MY-polymer reaches the edge of the mold it spreads around all the mold (capillary forces). Especially fluidic inlets at the sides support that unwanted effect. \Rightarrow check for MY-polymer-rests inside alignment-structures and optical elements and remove them with tweezers.

For **bonding**, MY-polymer-filled PDMS-parts and empty counterparts were rinsed in ethanol, activated in O₂-plasma (500 W, 80 mbar, 16sec) and aligned under optical microscope with water buffer to avoid immediate bonding. Aligned chips were dried in oven at 100°C. (*note: open the fluidic channels before bonding (!), alignment of interrogation-area doesn't mean coincidence of self-alignment channels, if no lenses are present.*)

C.2.2.3 Repetition of C.2.2: MY-polymer in pre-coated PDMS-mold, curing on glass

Fabrication of Hybrids, see C.2.2

1. replication of PDMS-molds
2. open fluidic channels

3. coating of PDMS-molds (face with channels) with Primer G using air-brush
4. superficial cleaning of coated surface with acetone-wetted cloth (this way leaving the inside of the channels coated)
5. stick coated PDMS-molds to clean glass-slides
 - after one hour still ok
 - *don't use any additional adhesion promotor, especially no liquids!* In the first attempt, which failed to cure MY-132 A, this was done in order to avoid air-inclusions, which eventually cumber the complete filling of the channels with MY-polymer. The liquid probably washed away the primer, which led to direct contact of MY-132 A with PDMS (silicone rubber, [see Datasheet](#)) during exposure. At the same time, MY-132 A was blur due to partly crystallization (theoretically crystallization-process can be reversed by heating to 60-70°C for 30min [see Datasheet](#), but here it didn't as proved afterwards in several attempts). Wich one of those factors inhibited polymerisation, is unclear. However, structures were found rather attached to the glass slide after exposure than to the PDMS.
6. add droplet of MY-133 V2000 at one fluidic inlet and wait until channels are complete filled
7. set samples under water and expose under UV-light (KS MA6) for 10min
8. remove samples from water; MY-polymer-structures should stay attached to PDMS-mold, no polymer-rests on glass-slides
9. check under microscope for primer-rests in optical elements and eventually remove them with tweezers
10. activate PDMS-surfaces of MY-polymer-filled structures and un-filled counterparts in O₂-plasma (18sec at 500 W and 80 mbar) attach to each other and align under microscope with water as buffer
11. dry on hotplate at 65°C

Particle scattering after Mie-theory

Theoretical scattering curves were calculated using the python wrapper module *py-mie 0.4.0* by Rothenberg and Hirsch which is based on the publications of Toon and Ackerman [1981], Moore [1998].

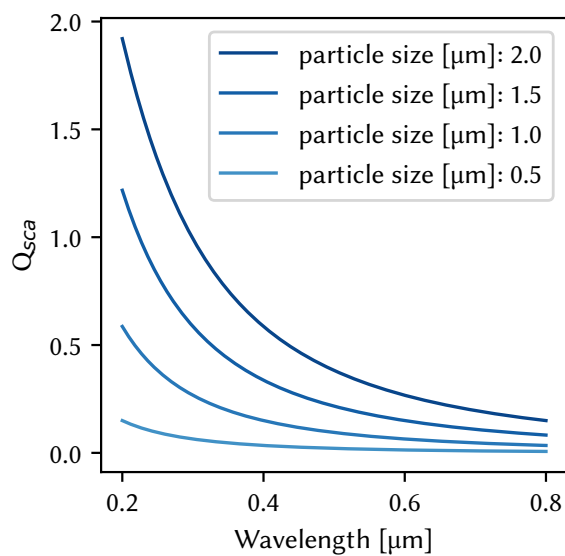


FIGURE D.1: Mie scattering of spheres with $n = 1.38$ submerged in water

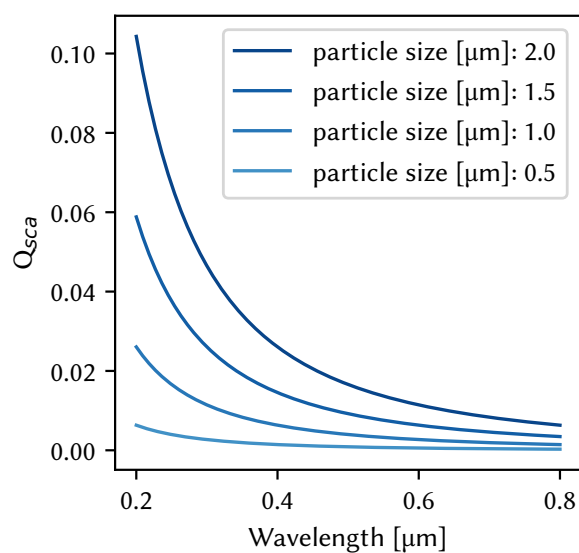


FIGURE D.2: Mie scattering of spheres with $n = 1.38$ submerged in medium with $n = 1.37$.

Bibliography

- Isaac Rodríguez-Ruiz, Mayte Conejero-Muriel, Tobias N. Ackermann, José A. Gavira, and Andreu Llobera. A multiple path photonic lab on a chip for parallel protein concentration measurements. In *Lab Chip*, volume 15, pages 1133–1139, 2015a. ISBN 9780979806476. doi: 10.1039/C4LC01332H. URL <http://xlink.rsc.org/?DOI=C4LC01332H>.
- Erik Stijns and Hugo Thienpont. *Fundamentals of Photonics*. Wiley Series in Pure and Applied Optics. John Wiley & Sons, Inc., New York, USA, aug 2011. ISBN 9783527409563. doi: 10.1002/9783527635245.ch2. URL <http://doi.wiley.com/10.1002/0471213748>.
- Victor Yashunsky, Tal Marciano, Vladislav Lirtsman, Michael Golosovsky, Dan Davidov, and Benjamin Aroeti. Real-Time Sensing of Cell Morphology by Infrared Waveguide Spectroscopy. *PLoS ONE*, 7(10):e48454, jan 2012. ISSN 19326203. doi: 10.1371/journal.pone.0048454. URL <http://www.pubmedcentral.nih.gov/articlerender.fcgi?artid=3485211&tool=pmcentrez&rendertype=abstract><http://dx.plos.org/10.1371/journal.pone.0048454>.
- Hongbao Xin, Yayi Li, Xiaoshuai Liu, and Baojun Li. Escherichia coli -based biophotonic waveguides. *Nano Letters*, 13(7):3408–3413, jun 2013. ISSN 15306984. doi: 10.1021/nl401870d.
- Erik Unosson. *Antibacterial strategies for titanium biomaterials*. PhD thesis, 2015.
- John D. Hunter. Matplotlib: A 2D graphics environment. *Computing in Science and Engineering*, 9(3):99–104, 2007. ISSN 15219615. doi: 10.1109/MCSE.2007.55.
- Eric K. Sackmann, Anna L. Fulton, and David J. Beebe. The present and future role of microfluidics in biomedical research. *Nature*, 507(7491):181–189, 2014. ISSN 0028-0836. doi: 10.1038/nature13118. URL <http://www.nature.com/doifinder/10.1038/nature13118>.
- Nathan Blow. Microfluidics: the great divide. *Nature Methods*, 6(9):683–686, 2009. ISSN 1548-7091. doi: 10.1038/nmeth0909-683. URL <http://www.nature.com/doifinder/10.1038/nmeth0909-683>.
- Holger Becker. Hype, hope and hubris: the quest for the killer application in microfluidics. *Lab on a Chip*, 9(15):2119, 2009. ISSN 1473-0197. doi: 10.1039/b911553f. URL <http://xlink.rsc.org/?DOI=b911553f>.
- D. Mark, S. Haeberle, G. Roth, F. Von Stetten, and R. Zengerle. Microfluidic lab-on-a-chip platforms: Requirements, characteristics and applications. *NATO Science for Peace and Security Series A: Chemistry and Biology*, 39(3):305–376, 2010. ISSN 18746489. doi: 10.1007/

978-90-481-9029-4-17. URL <http://pubs.rsc.org/en/content/articlehtml/2010/cs/b820557b>.

Lisa R. Volpatti and Ali K. Yetisen. Commercialization of microfluidic devices. *Trends in Biotechnology*, 32(7):347–350, 2014. ISSN 18793096. doi: 10.1016/j.tibtech.2014.04.010. URL <http://dx.doi.org/10.1016/j.tibtech.2014.04.010>.

Sangeeta N Bhatia and Donald E Ingber. Microfluidic organs-on-chips. *Nature Biotechnology*, 32(8):760–772, 2014. ISSN 1087-0156. doi: 10.1038/nbt.2989. URL <http://www.nature.com/doifinder/10.1038/nbt.2989>.

A. Manz, N. Graber, and H. M. Widmer. Miniaturized total chemical analysis systems: A novel concept for chemical sensing. *Sensors and Actuators: B. Chemical*, 1(1-6):244–248, 1990. ISSN 09254005. doi: 10.1016/0925-4005(90)80209-I. URL <http://linkinghub.elsevier.com/retrieve/pii/092540059080209I>.

David J. Beebe, Glennys A. Mensing, and Glenn M. Walker. Physics and Applications of Microfluidics in Biology. *Annual Review of Biomedical Engineering*, 4(1):261–286, 2002. ISSN 1523-9829. doi: 10.1146/annurev.bioeng.4.112601.125916. URL <http://www.annualreviews.org/doi/10.1146/annurev.bioeng.4.112601.125916>.

Carsten Haber. Microfluidics in commercial applications; an industry perspective. *Lab on a Chip*, 6(9):1118, 2006. ISSN 1473-0197. doi: 10.1039/b610250f. URL <http://xlink.rsc.org/?DOI=b610250f>.

D J Laser and J G Santiago. A review of micropumps. *Journal of Micromechanics and Microengineering*, 14(6):R35–R64, 2004. ISSN 0960-1317. doi: 10.1088/0960-1317/14/6/R01. URL <http://stacks.iop.org/0960-1317/14/i=6/a=R01?key=crossref.137857bfcf5ea513064ec576b484af8f>.

Peter Woias. Micropumps - Past, progress and future prospects. *Sensors and Actuators, B: Chemical*, 105(1):28–38, 2005. ISSN 09254005. doi: 10.1016/j.snb.2004.02.033.

Kwang W Oh and Chong H Ahn. A review of microvalves. *Journal of Micromechanics and Microengineering*, 16(5):R13–R39, 2006. ISSN 0960-1317. doi: 10.1088/0960-1317/16/5/R01. URL <http://stacks.iop.org/0960-1317/16/i=5/a=R01?key=crossref.c5cf9020613ed3137ffb01175e1871b7>.

- Volker Hessel, Holger Löwe, and Friedhelm Schönfeld. Micromixers - A review on passive and active mixing principles. *Chemical Engineering Science*, 60(8-9 SPEC. ISS.):2479–2501, 2005. ISSN 00092509. doi: 10.1016/j.ces.2004.11.033.
- Nam-Trung Nguyen and Zhigang Wu. Micromixers—a review. *Journal of Micromechanics and Microengineering*, 15(2):R1–R16, 2005. ISSN 0960-1317. doi: 10.1088/0960-1317/15/2/R01. URL <http://stacks.iop.org/0960-1317/15/i=2/a=R01?key=crossref.0cc4282f2ae2efd83949fe482c71c476>.
- Chia Yen Lee, Chin Lung Chang, Yao Nan Wang, and Lung Ming Fu. Microfluidic mixing: A review. *International Journal of Molecular Sciences*, 12(5):3263–3287, 2011. ISSN 14220067. doi: 10.3390/ijms12053263.
- David M. Cate, Jaclyn A. Adkins, Jaruwat Mettakoonpitak, and Charles S. Henry. Recent developments in paper-based microfluidic devices. *Analytical Chemistry*, 87(1):19–41, 2015. ISSN 15206882. doi: 10.1021/ac503968p.
- Darius G. Rackus, Mohtashim H. Shamsi, and Aaron R. Wheeler. Electrochemistry, biosensors and microfluidics: a convergence of fields. *Chem. Soc. Rev.*, 44(15):5320–5340, 2015. ISSN 0306-0012. doi: 10.1039/C4CS00369A. URL <http://xlink.rsc.org/?DOI=C4CS00369A>.
- Bambang Kuswandi, Nuriman, Jurriaan Huskens, and Willem Verboom. Optical sensing systems for microfluidic devices: A review. *Analytica Chimica Acta*, 601(2):141–155, oct 2007. ISSN 00032670. doi: 10.1016/j.aca.2007.08.046. URL <http://linkinghub.elsevier.com/retrieve/pii/S0003267007014444>.
- Klaus B. Mogensen and Jörg P. Kutter. Optical detection in microfluidic systems. *Electrophoresis*, 30(SUPPL. 1):92–100, 2009. ISSN 01730835. doi: 10.1002/elps.200900101.
- M.C. Estevez, M. Alvarez, and L.M. Lechuga. Integrated optical devices for lab-on-a-chip biosensing applications. *Laser & Photonics Reviews*, 6(4):463–487, 2012. ISSN 18638880. doi: 10.1002/lpor.201100025. URL <http://doi.wiley.com/10.1002/lpor.201100025>.
- George M. Whitesides. The origins and the future of microfluidics. *Nature*, 442(7101):368–373, 2006. ISSN 0028-0836. doi: 10.1038/nature05058. URL <http://www.nature.com/doifinder/10.1038/nature05058>.
- Nuno Miguel Matos Pires, Tao Dong, Ulrik Hanke, and Nils Hoivik. Recent developments in optical detection technologies in lab-on-a-chip devices for biosensing applications. *Sensors*

- (Switzerland), 14(8):15458–15479, 2014. ISSN 14248220. doi: 10.3390/s140815458. URL <http://www.mdpi.com/1424-8220/14/8/15458/>.
- Isaac Rodríguez-Ruiz, Tobias N. Ackermann, Xavier Muñoz-Berbel, and Andreu Llobera. Photonic Lab-on-a-Chip: Integration of Optical Spectroscopy in Microfluidic Systems. *Analytical Chemistry*, 88(13):6630–6637, 2016. ISSN 15206882. doi: 10.1021/acs.analchem.6b00377. URL <http://dx.doi.org/10.1021/acs.analchem.6b00377>.
- P. K. Tien. Integrated optics and new wave phenomena in optical waveguides. *Reviews of Modern Physics*, 49(2):361–420, 1977. ISSN 00346861. doi: 10.1103/RevModPhys.49.361.
- David Holmes, Hywel Morgan, and Nicolas G. Green. High throughput particle analysis: Combining dielectrophoretic particle focussing with confocal optical detection. *Biosensors and Bioelectronics*, 21(8):1621–1630, 2006. ISSN 09565663. doi: 10.1016/j.bios.2005.10.017.
- David Barat, Giuseppe Benazzi, Matthew Charles Mowlem, Jesus Miguel Ruano, and Hywel Morgan. Design, simulation and characterisation of integrated optics for a microfabricated flow cytometer. *Optics Communications*, 283(9):1987–1992, 2010. ISSN 00304018. doi: 10.1016/j.optcom.2009.12.046.
- Joel P. Golden, Jason S. Kim, Jeffrey S. Erickson, Lisa R. Hilliard, Peter B. Howell, George P. Anderson, Mansoor Nasir, and Frances S. Ligler. Multi-wavelength microflow cytometer using groove-generated sheath flow. *Lab on a Chip*, 9(13):1942, 2009. ISSN 1473-0197. doi: 10.1039/b822442k. URL <http://xlink.rsc.org/?DOI=b822442k>.
- Robert Horváth, Henrik C Pedersen, Nina Skivesen, Christer Svanberg, and Niels B Larsen. Fabrication of reverse symmetry polymer waveguide sensor chips on nanoporous substrates using dip-floating. *Journal of Micromechanics and Microengineering*, 15(6):1260–1264, 2005. ISSN 0960-1317. doi: 10.1088/0960-1317/15/6/017.
- S. Balslev, A. M. Jorgensen, B. Bilenberg, K. B. Mogensen, D. Snakenborg, O. Geschke, J. P. Kutter, and A. Kristensen. Lab-on-a-chip with integrated optical transducers. *Lab Chip*, 6(2):213–217, 2006. ISSN 1473-0197. doi: 10.1039/B512546D. URL <http://xlink.rsc.org/?DOI=B512546D>.
- Xuhua Wang, Maliwan Amatatongchai, Duangjai Nacapricha, Oliver Hofmann, John C. de Mello, Donal D C Bradley, and Andrew J. de Mello. Thin-film organic photodiodes for integrated on-chip chemiluminescence detection - application to antioxidant capacity screening. *Sensors and Actuators, B: Chemical*, 140(2):643–648, 2009. ISSN 09254005. doi: 10.1016/j.snb.2009.04.068.

- Andreu Llobera, Joan Juvert, Alfredo González-Fernández, Bergoi Ibarlucea, Ester Carregal-Romero, Stephanus Büttgenbach, and César Fernández-Sánchez. Biofunctionalized all-polymer photonic lab on a chip with integrated solid-state light emitter. *Light: Science & Applications*, 4(4):e271, apr 2015. ISSN 2047-7538. doi: 10.1038/lssa.2015.44. URL <http://www.nature.com/doifinder/10.1038/lssa.2015.44>.
- G. de Cesare, A. Nascetti, R. Scipinotti, A. Zahra, and D. Caputo. On-chip detection performed by amorphous silicon balanced photosensor for lab-on chip application. *Sensing and Bio-Sensing Research*, 3:53–58, 2015. ISSN 22141804. doi: 10.1016/j.sbsr.2014.12.005. URL <http://linkinghub.elsevier.com/retrieve/pii/S2214180414000464>.
- S. Camou, H. Fujita, and T. Fujii. PDMS 2D optical lens integrated with microfluidic channels: principle and characterization. *Lab on a Chip*, 3(1):40, 2003. ISSN 1473-0197. doi: 10.1039/b211280a. URL <http://xlink.rsc.org/?DOI=b211280a>.
- Suz Kai Hsiung, Che Hsin Lin, and Gwo Bin Lee. A microfabricated capillary electrophoresis chip with multiple buried optical fibers and microfocusing lens for multiwavelength detection. *Electrophoresis*, 26(6):1122–1129, 2005. ISSN 01730835. doi: 10.1002/elps.200410034.
- Suz Kai Hsiung, Gwo Bin Lee, Che Hsin Lin, and Chun Hong Lee. Microcapillary Electrophoresis Chip Device Integrated with Micro Focusing Lens Structures and Its Biomedical Applications. *Fooyin Journal of Health Sciences*, 1(1):11–20, 2009. ISSN 18778607. doi: 10.1016/S1877-8607(09)60003-5.
- Jeonggi Seo and Luke P. Lee. Disposable integrated microfluidics with self-aligned planar microlenses. *Sensors and Actuators, B: Chemical*, 99(2-3):615–622, 2004. ISSN 09254005. doi: 10.1016/j.snb.2003.11.014.
- Jordi Vila-Planas, Elisabet Fernández-Rosas, Bergoi Ibarlucea, Stefanie Demming, Carme Nogués, Jose A Plaza, Carlos Domínguez, Stephanus Büttgenbach, and Andreu Llobera. Cell analysis using a multiple internal reflection photonic lab-on-a-chip. *Nature Protocols*, 6(10):1642–1655, 2011. ISSN 1754-2189. doi: 10.1038/nprot.2011.383. URL <http://www.nature.com/doifinder/10.1038/nprot.2011.383>.
- Isaac Rodríguez-Ruiz, Sébastien Teychené, Nhat Van Pham, Dimitri Radajewski, Fabrice Lamadie, Andreu Llobera, and Sophie Charton. Broadcasting photonic lab on a chip concept through a low cost manufacturing approach. *Talanta*, 170(April):180–184, 2017. ISSN 00399140. doi: 10.1016/j.talanta.2017.04.010.

- Carl K. Fredrickson and Z. Hugh Fan. Macro-to-micro interfaces for microfluidic devices. *Lab on a Chip*, 4(6):526, 2004. ISSN 1473-0197. doi: 10.1039/b410720a. URL <http://xlink.rsc.org/?DOI=b410720a>.
- Mazher Iqbal Mohammed, Steven Haswell, and Ian Gibson. Lab-on-a-chip or Chip-in-a-lab: Challenges of Commercialization Lost in Translation. *Procedia Technology*, 20(July):54–59, 2015. ISSN 22120173. doi: 10.1016/j.protcy.2015.07.010. URL <http://linkinghub.elsevier.com/retrieve/pii/S2212017315001875>.
- Elisabeth Wilhelm, Christiane Neumann, Thomas Duttonhofer, Leonardo Pires, and Bastian E. Rapp. Connecting microfluidic chips using a chemically inert, reversible, multichannel chip-to-world-interface. *Lab on a Chip*, 13(22):4343, 2013. ISSN 1473-0197. doi: 10.1039/c3lc50861g. URL <http://xlink.rsc.org/?DOI=c3lc50861g>.
- Dirk van Swaay, Jean-Pierre Mächler, Claire Stanley, and Andrew DeMello. A chip-to-world connector with a built-in reservoir for simple small-volume sample injection. *Lab Chip*, 14(1):178–181, 2014. ISSN 1473-0197. doi: 10.1039/C3LC51065D. URL <http://xlink.rsc.org/?DOI=C3LC51065D>.
- Yuksel Temiz, Robert D. Lovchik, Govind V. Kaigala, and Emmanuel Delamarche. Lab-on-a-chip devices: How to close and plug the lab? *Microelectronic Engineering*, 132:156–175, 2015. ISSN 01679317. doi: 10.1016/j.mee.2014.10.013. URL <http://linkinghub.elsevier.com/retrieve/pii/S0167931714004456>.
- Greg Szulczewski, Stefano Sanvito, and Michael Coey. A spin of their own. *Nature Materials*, 8(9):693–695, 2009. ISSN 1476-1122. doi: 10.1038/nmat2518. URL <http://www.nature.com/doi/10.1038/nmat2518>.
- Long Que. *2.03 - Thermal Actuation*. Elsevier, Boston, MA, 2008. ISBN 978-0-444-52190-3. doi: <http://dx.doi.org/10.1016/B978-044452190-3.00060-4>. URL <http://www.sciencedirect.com/science/article/pii/B9780444521903000604>.
- K. Y. Lee. Micromachining applications of a high resolution ultrathick photoresist. *Journal of Vacuum Science & Technology B: Microelectronics and Nanometer Structures*, 13(6):3012, 1995. ISSN 0734211X. doi: 10.1116/1.588297. URL <http://scitation.aip.org/content/avs/journal/jvstb/13/6/10.1116/1.588297>.
- Younan Xia and George M. Whitesides. Soft Lithography. *Annual Review of Materials Science*, 28(1):153–184, 1998. ISSN 0084-6600. doi: 10.1146/annurev.matsci.28.1.153. URL <http://www.annualreviews.org/doi/10.1146/annurev.matsci.28.1.153>.

- Shashi Prakash and Subrata Kumar. Fabrication of microchannels on transparent PMMA using CO₂ Laser (10.6 μ m) for microfluidic applications: An experimental investigation. *International Journal of Precision Engineering and Manufacturing*, 16(2):361–366, 2015. ISSN 20054602. doi: 10.1007/s12541-015-0047-8. URL <http://link.springer.com/10.1007/s12541-015-0047-8>.
- Eugene Hecht. *Optics (4th Edition)*. Addison Wesley, 4 edition, aug 2001. ISBN 0805385665. URL <http://www.worldcat.org/isbn/0805385665>.
- Thomas C. Vogelmann. Plant Tissue Optics. *Annual Review of Plant Physiology and Plant Molecular Biology*, 44(1):231–251, 1993. ISSN 1040-2519. doi: 10.1146/annurev.pp.44.060193.001311.
- K. Franze, J. Grosche, S. N. Skatchkov, S. Schinkinger, C. Foja, D. Schild, O. Uckermann, K. Travis, A. Reichenbach, and J. Guck. Muller cells are living optical fibers in the vertebrate retina. *Proceedings of the National Academy of Sciences*, 104(20):8287–8292, 2007. ISSN 0027-8424. doi: 10.1073/pnas.0611180104. URL <http://www.pnas.org/cgi/doi/10.1073/pnas.0611180104>.
- J. Aizenberg, V. C. Sundar, A. D. Yablon, J. C. Weaver, and G. Chen. Biological glass fibers: Correlation between optical and structural properties. *Proceedings of the National Academy of Sciences*, 101(10):3358–3363, 2004. ISSN 0027-8424. doi: 10.1073/pnas.0307843101. URL <http://www.pnas.org/cgi/doi/10.1073/pnas.0307843101>.
- Nathan Blow. Microfluidics: in search of a killer application. *Nature Methods*, 4(8):665–670, 2007. ISSN 1548-7091. doi: 10.1038/nmeth0807-665. URL <http://www.nature.com/doifinder/10.1038/nmeth0807-665>.
- Tobias Nils Ackermann, Pablo Giménez-Gómez, Xavier Muñoz-Berbel, and Andreu Llobera. Plug and measure – a chip-to-world interface for photonic lab-on-a-chip applications. *Lab Chip*, 16(17):3220–3226, 2016a. ISSN 1473-0197. doi: 10.1039/C6LC00462H. URL <http://xlink.rsc.org/?DOI=C6LC00462H>.
- Amit Prabhakar and Soumyo Mukherji. C-shaped embedded polymer waveguide for evanescent field absorption based lab on a chip biosensor. *International Conference on Systems in Medicine and Biology, ICSMB 2010 - Proceedings*, pages 67–70, 2010. ISSN 1473-0197. doi: 10.1109/ICSMB.2010.5735347.
- Benjamin R. Watts, Zhiyi Zhang, Chang-Qing Xu, Xudong Cao, and Min Lin. Integration of optical components on-chip for scattering and fluorescence detection in an optofluidic device.

- Biomedical Optics Express*, 3(11):2784, 2012. ISSN 2156-7085. doi: 10.1364/BOE.3.002784. URL <https://www.osapublishing.org/boe/abstract.cfm?uri=boe-3-11-2784>.
- Peng Fei, Zitian Chen, Yongfan Men, Ang Li, Yiran Shen, and Yanyi Huang. A compact optofluidic cytometer with integrated liquid-core/PDMS-cladding waveguides. *Lab on a Chip*, 12(19):3700, 2012. ISSN 1473-0197. doi: 10.1039/c2lc40329c. URL <http://xlink.rsc.org/?DOI=c2lc40329c>.
- Jessica Godin, Chun Hao Chen, Sung Hwan Cho, Wen Qiao, Frank Tsai, and Yu Hwa Lo. Microfluidics and photonics for bio-System-on-a-Chip: A review of advancements in technology towards a microfluidic flow cytometry chip. *Journal of Biophotonics*, 1(5):355–376, 2008. ISSN 1864063X. doi: 10.1002/jbio.200810018.
- Jessica Godin, Victor Lien, and Yu Hwa Lo. Demonstration of two-dimensional fluidic lens for integration into microfluidic flow cytometers. *Applied Physics Letters*, 89(6):2006–2008, 2006. ISSN 00036951. doi: 10.1063/1.2266887.
- Z. Wang, J. El-Ali, M. Engelund, T. Gotsæd, I. R. Perch-Nielsen, K. B. Mogensen, D. Snakenborg, J. P. Kutter, and A. Wolff. Measurements of scattered light on a microchip flow cytometer with integrated polymer based optical elements. *Lab Chip*, 4(4):372–377, aug 2004. ISSN 1473-0197. doi: 10.1039/B400663A. URL <http://xlink.rsc.org/?DOI=B400663A>.
- Tobias Wienhold, Sarah Kraemmer, Andreas Bacher, Heinz Kalt, Christian Koos, Sebastian Koeber, and Timo Mappes. Efficient free-space read-out of WGM lasers using circular micromirrors. *Optics Express*, 23(2):1025, 2015. ISSN 1094-4087. doi: 10.1364/OE.23.001025. URL <https://www.osapublishing.org/abstract.cfm?URI=oe-23-2-1025>.
- Uwe Bog, Falko Brinkmann, Sentayehu Fetene Wondimu, Tobias Wienhold, Sarah Kraemmer, Christian Koos, Heinz Kalt, Michael Hirtz, Harald Fuchs, Sebastian Koeber, and Timo Mappes. Densely Packed Microgoblet Laser Pairs for Cross-Referenced Biomolecular Detection. *Advanced Science*, 2(10):1–6, 2015. ISSN 21983844. doi: 10.1002/advs.201500066. URL <http://dx.doi.org/10.1002/advs.201500066>.
- Luanne Hall-Stoodley, J. William Costerton, and Paul Stoodley. Bacterial biofilms: from the Natural environment to infectious diseases. *Nature Reviews Microbiology*, 2(2):95–108, 2004. ISSN 1740-1526. doi: 10.1038/nrmicro821. URL <http://www.nature.com/doifinder/10.1038/nrmicro821>.
- David L Popham, M E Gilmore, and Peter Setlow. *Current research and applications*. Caister Academic Press, 2012. ISBN 1904455964\9781904455967.

Søren Molin and Tim Tolker-Nielsen. Gene transfer occurs with enhanced efficiency in biofilms and induces enhanced stabilisation of the biofilm structure, 2003. ISSN 09581669.

Philip S. Stewart. Mechanisms of antibiotic resistance in bacterial biofilms. *International Journal of Medical Microbiology*, 292(2):107–113, 2002. ISSN 14384221. doi: 10.1078/1438-4221-00196. URL <http://linkinghub.elsevier.com/retrieve/pii/S1438422104700909>.

R. Murga, T. S. Forster, E. Brown, J. M. Pruckler, B. S. Fields, and R. M. Donlan. Role of biofilms in the survival of *Legionella pneumophila* in a model potable-water system. *Microbiology*, 147(11):3121–3126, 2001. ISSN 13500872. doi: 10.1099/00221287-147-11-3121.

Dingding An and Matthew R. Parsek. The promise and peril of transcriptional profiling in biofilm communities, 2007. ISSN 13695274.

C. B. Whitchurch. Extracellular DNA Required for Bacterial Biofilm Formation. *Science*, 295(5559):1487–1487, 2002. ISSN 00368075. doi: 10.1126/science.295.5559.1487. URL <http://www.sciencemag.org/cgi/doi/10.1126/science.295.5559.1487>.

B Bilenberg, T Nielsen, B Clausen, and A Kristensen. PMMA to SU-8 bonding for polymer based lab-on-a-chip systems with integrated optics. *Journal of Micromechanics and Microengineering*, 14(6):814–818, 2004. ISSN 0960-1317. doi: 10.1088/0960-1317/14/6/008. URL <http://stacks.iop.org/0960-1317/14/i=6/a=008?key=crossref.e1dab429077b9f1fb5f97c47e5093047>.

T. Q. TRUONG and N. T. NGUYEN. Su-8 on Pmma – a New Technology for Microfluidics. *International Journal of Computational Engineering Science*, 04(03):667–670, 2003. ISSN 1465-8763. doi: 10.1142/S1465876303002003. URL <http://www.worldscientific.com/doi/abs/10.1142/S1465876303002003>.

Andrea Bubendorfer, Xianming Liu, and Amanda V Ellis. Microfabrication of PDMS microchannels using SU-8/PMMA moldings and their sealing to polystyrene substrates. *Smart Materials and Structures*, 16(2):367–371, 2007. ISSN 0964-1726. doi: 10.1088/0964-1726/16/2/015. URL <http://stacks.iop.org/0964-1726/16/i=2/a=015?key=crossref.0f94d8cec797d8a65849351247673b43>.

Brian J Kim and Ellis Meng. Review of polymer MEMS micromachining. *Journal of Micromechanics and Microengineering*, 26(1):013001, 2016. ISSN 0960-1317. doi: 10.1088/0960-1317/26/1/013001. URL <http://stacks.iop.org/0960-1317/26/i=1/a=013001?key=crossref.c5b3025495e9716ab0088134ccf07264>.

- M P Larsson, R R A Syms, and A G Wojcik. Improved adhesion in hybrid Si-polymer MEMS via micromechanical interlocking. *Journal of Micromechanics and Microengineering*, 15(11):2074–2082, 2005. ISSN 0960-1317. doi: 10.1088/0960-1317/15/11/012. URL <http://stacks.iop.org/0960-1317/15/i=11/a=012?key=crossref.0450c1dfb8cd75b02df1480c9d27a2da>.
- Alireza Shamsi, Ali Amiri, Payam Heydari, Hasan Hajghasem, Mansour Mohtashamifar, and Mehrnaz Esfandiari. Low cost method for hot embossing of microstructures on PMMA by SU-8 masters. *Microsystem Technologies*, 20(10-11):1925–1931, oct 2014. ISSN 09467076. doi: 10.1007/s00542-013-2000-z. URL <http://link.springer.com/10.1007/s00542-013-2000-z>.
- E. Karatan and P. Watnick. Signals, Regulatory Networks, and Materials That Build and Break Bacterial Biofilms. *Microbiology and Molecular Biology Reviews*, 73(2):310–347, 2009. ISSN 1092-2172. doi: 10.1128/MMBR.00041-08. URL <http://mmbbr.asm.org/cgi/doi/10.1128/MMBR.00041-08>.
- I H Malitson. Interspecimen Comparison of the Refractive Index of Fused Silica. *J. Opt. Soc. Am.*, 55(10):1205–1209, oct 1965. doi: 10.1364/JOSA.55.001205. URL <http://www.osapublishing.org/abstract.cfm?URI=josa-55-10-1205>.
- N. Sultanova, S. Kasarova, and I. Nikolov. Dispersion properties of optical polymers. In *Acta Physica Polonica A*, volume 116, pages 585–587, 2009. ISBN 05874246. doi: 10.12693/APhysPolA.116.585.
- EOC. MY polymers; bio-medical, 2013. URL <http://www.eoc-inc.com/MY-Polymers/bio-medicalapplications.pdf>.
- P. Karasiński. Influence of aging and annealing on the properties of silica films produced with sol-gel method. *Optica Applicata*, 36(2-3):389–399, 2006. ISSN 00785466.
- Paweł Karasiński, Janusz Jaglarz, Manuela Reben, Edyta Skoczek, and Jacek Mazur. Porous silica xerogel films as antireflective coatings - Fabrication and characterization. *Optical Materials*, 33(12):1989–1994, oct 2011. ISSN 09253467. doi: 10.1016/j.optmat.2011.04.003. URL <http://linkinghub.elsevier.com/retrieve/pii/S0925346711002072>.
- Martin R. Bennett, Sanjay Sinha, and Gary K. Owens. Vascular Smooth Muscle Cells in Atherosclerosis. *Circulation Research*, 118(4):692–702, 2016. ISSN 15244571. doi: 10.1161/CIRCRESAHA.115.306361.

- Stephen P Evanko, John C Angello, Thomas N Wight, Stephen P Evanko, John C Angello, and Thomas N Wight. Vascular Smooth Muscle Cells. *Methods in Molecular Medicine*, 46(6):237–245, 1999.
- Cristina Rius, Tobias N. Ackermann, Beatriz Dorado, Xavier Muñoz-Berbel, Vicente Andrés, and Andreu Llobera. Fiber optic label-free biophotonic diagnostic tool for cardiovascular disease. In Sander van den Driesche, editor, *Progress in Biomedical Optics and Imaging - Proceedings of SPIE*, volume 9518, page 95180V. SPIE, jun 2015. ISBN 9781628416411. doi: 10.1117/12.2179062. URL <http://proceedings.spiedigitallibrary.org/proceeding.aspx?doi=10.1117/12.2179062>.
- D. King, E. Røge Hedegaard, Tobias Nils Ackermann, C. Rius, X. Muñoz-Berbel, H. Knudsen, I. Rodríguez-Rodríguez, B. Dorado, E. Alvarez, J. Ducrée, V. Andrés, U. Simonsen, and A. Llobera. Living photonics: Monitoring light propagation through cells (LiPhos). *Progress in Biomedical Optics and Imaging - Proceedings of SPIE*, 9518:1–7, 2015. ISSN 16057422. doi: <http://dx.doi.org/10.1117/12.2181306>.
- S de Pedro, V J Cadarso, T N Ackermann, X Muñoz-Berbel, J A Plaza, J Brugger, S Büttgenbach, and A Llobera. Polymeric variable optical attenuators based on magnetic sensitive stimuli materials. *Journal of Micromechanics and Microengineering*, 24(12):125008, dec 2014. ISSN 0960-1317. doi: 10.1088/0960-1317/24/12/125008. URL <http://www.scopus.com/inward/record.url?eid=2-s2.0-84914693659&partnerID=tZOtx3y1>.
- David Sanahuja, Pablo Gimenez-Gomez, Nuria Vignes, Tobias Nils Ackermann, Alfons Eduard Guerrero-Navarro, Ferran Pujol-Vila, Jordi Sacristan, Nidia Santamaria, Maria Sanchez-Contreras, Maria Diaz-Gonzalez, Jordi Mas, and Xavier Munoz-Berbel. Microbial trench-based optofluidic system for reagentless determination of phenolic compounds. *Lab on a chip*, 15(7):1717–1726, 2015. ISSN 1473-0189 (Electronic). doi: 10.1039/c4lc01446d. URL <http://dx.doi.org/10.1039/C4LC01446D>.
- Isaac Rodríguez-Ruiz, Eduard Masvidal-Codina, Tobias Nils Ackermann, and Andreu Llobera. Photonic lab-on-chip (PhLOC) for enzyme-catalyzed reactions in continuous flow. *Microfluidics and Nanofluidics*, 18(5-6):1277–1286, 2015b. ISSN 1613-4982. URL <http://dx.doi.org/10.1007/s10404-014-1526-4>.
- Ryo Usuba, Masatoshi Yokokawa, Tobias Nils Ackermann, Andreu Llobera, Kiyoshi Fukunaga, Soichiro Murata, Nobuhiro Ohkohchi, and Hiroaki Suzuki. Photonic Lab-on-a-Chip for Rapid Cytokine Detection. *ACS Sensors*, 1(8):979–986, 2016. ISSN 23793694. doi: 10.1021/acssensors.6b00193. URL <http://dx.doi.org/10.1021/acssensors.6b00193>.

Sandra De Pedro, Tobias N. Ackermann, Jose A. Plaza, Erica Alvarez, Stephanus Büttgenbach, Victor J. Cadarso, and Andreu Llobera. All-photonic SU-8 Variable Optical Attenuator. In *International Conference on Optical MEMS and Nanophotonics*, pages 63–64. IEEE, aug 2014. ISBN 9780992841423. doi: 10.1109/OMN.2014.6924544. URL <http://dx.doi.org/10.1109/OMN.2014.6924544>.

Tobias N Ackermann, Jordi Vila-planas, Xavier Muñoz-berbel, Erica Álvarez-conde, Daniel Kopp, Hans Zappe, and Andreu Llobera. Modular optofluidic systems : A toolbox for fast and simple assembly of a photonic lab on a chip . pages 21–22, San Jose, California (USA), 2016b. CLEO:2016. ISBN 9781943580118.

Tobias N. Ackermann, Jiri Dietvorst, Ana Sanchis, Juan P. Salvador, Xavier Munoz-Berbel, Erica Alvarez-Conde, Daniel Kopp, Hans Zappe, M.-Pilar Marco, and Andreu Llobera. Modular Optofluidic Systems (MOPS). In *μTAS 2014, San Antonio Texas*, page 100131C, 2016c. ISBN 9780979806476. doi: 10.1117/12.2242997. URL <http://proceedings.spiedigitallibrary.org/proceeding.aspx?doi=10.1117/12.2242997>.

Daniel Rothenberg and Thomas Hirsch. darothen/py-mie: py-mie 0.4.0. Zenodo. URL <http://doi.org/10.5281/zenodo.192510>.

Owen B. Toon and T. P. Ackerman. Algorithms for the calculation of scattering by stratified spheres. *Applied Optics*, 20(20):3657–3660, 1981. ISSN 0003-6935. doi: 10.1364/AO.20.003657.

Toby Moore. ABSORPTION AND SCATTERING OF LIGHT BY SMALL PARTICLES by C.F. Bohren and D.R. Huffman, Wiley Science Paperback Series, Chichester, UK, 1998, xiv+530 pp., List of references, index (£34.95; pbk), 1998. ISSN 02635747. URL <http://adsabs.harvard.edu/abs/1983uaz...rept....B>.